Dynamic Crack Propagation Analysis in DCB Specimen by using Cohesive Zone Modeling Technique

A Thesis Submitted
in Partial Fulfillment of the Requirements
for the Degree of

Master of Technology

by

Pradeep Kumar Yadav

DEPARTMENT OF MECHANICAL ENGINEERING

INDIAN INSTITUTE OF TECHNOLOGY, KANPUR

JUNE, 2005

TH
ME/2005/M
Y11

12 JUL 2005/ME
पुरुषोत्तम काशीनाथ केलकर पुस्तकालय
भारतीय प्रौद्योगिकी संस्थान कानपुर
क्रमांक सं० A..152023

A152023

CERTIFICATE

It is certified that the work contained in the thesis entitled "**DYNAMIC CRACK PROPAGATION ANALYSIS IN DCB SPECIMEN BY USING COHESIVE ZONE MODELING TECHNIQUE** " by PRADEEP KUMAR YADAV has been carried out under my supervision and this work has not been submitted elsewhere for a degree.

N N Kishore

Date: Professor N. N. Kishore '15

Department of Mechanical Engineering

Indian Institute of Technology, Kanpur

Kanpur, 208016

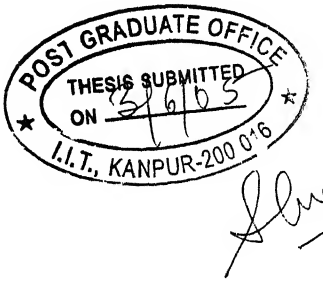

ACKNOWLEDGEMENTS

I take this opportunity to express my immense gratitude to Dr. N. N. Kishore for his invaluable guidance, numerous discussions and suggestions, constant encouragement, patient listening that he gave to my problems, and for all the knowledge that I have acquired from him. His friendly way of interacting and systematic approach made the work enjoyable. I am indebted to him for encouraging me to work on new approaches related to FEM.

I would like to express my deep sense of love and gratitude for my institute, the Indian Institute of Technology, Kanpur. This work would not have been possible without the excellent facilities provided by the institute; the computational facilities, the digital subscription of journals and the grand central library. The beautiful work culture, high learning rate and overall atmosphere of the campus have brought significant improvements in my personality, attitude and thinking.

I express my sincere thanks to my lab-mates Prashant, Alok, Vijay and Pankaj for their support. Special thanks to Mr. A.K.Singh and Mr. Mukul Shukla for his timely help during lab-work.

I express my special thanks to my friends Vinod, Nitin and Ritesh for all their affection, help and support that they extended to me during my two-year stay at IITK.

Finally, I thank the Almighty for always showing me the right path and providing me the strength and courage to move on.

June 2005 Pradeep Kumar Yadav

Indian Institute of Technology, Kanpur

ABSTRACT

The phenomenon of dynamic fracture is of interest in a wide variety of contexts from high speed manufacturing and defence applications to geophysics and seismology. The formulation and analytical solutions of dynamic fracture problems are very complex. Experimental and numerical methods like finite element methods are used extensively for solving dynamic fracture problems. In present work an attempt is made to simulate the dynamic crack propagation in DCB specimen by using the Cohesive Zone Model technique.

The interface crack problem is modeled by using cohesive zone theory. Cohesive zone theory takes into account various inelastic processes in the process zone existing ahead of crack tip. The cohesive zone model characterized by quadratic traction separation law is used to model the cohesive zone. A two dimensional plain strain formulation is employed for the analysis. For discretization of the cohesive zone interface cohesive elements are used.

The finite element model is first validated with hypothetical data for isotropic DCB specimen. Results give smooth variation of energy release rate curve. This method is also applied to the experimental data on glass fabric/epoxy composites. Results shows that the energy release rate gives fairly smooth variation.

Contents

List of Figures

List of Tables

Chapter 1

Introduction

1.1 General Introduction

Composite materials are the choice as well as the need of the present world. Their popularity is due to their inherent properties such as high strength to weight ratio, and most important, controllable anisotropy i.e. different strength levels can be achieved in different directions according to the need.

Mechanically fastened joints are critical parts in composite aerospace applications. The material combination in joined parts, along with stress concentration around the hole, makes a joint very complex element to design. Predicting strength of these parts is of great practical interest. Hence it is worthwhile to investigate into failure modes in mechanically fastened composite structures. Composite material with mechanical fasteners is commonly susceptible to the following modes of failure:

1. Bearing
2. Tension
3. Shear out
4. Pull out
5. Delamination

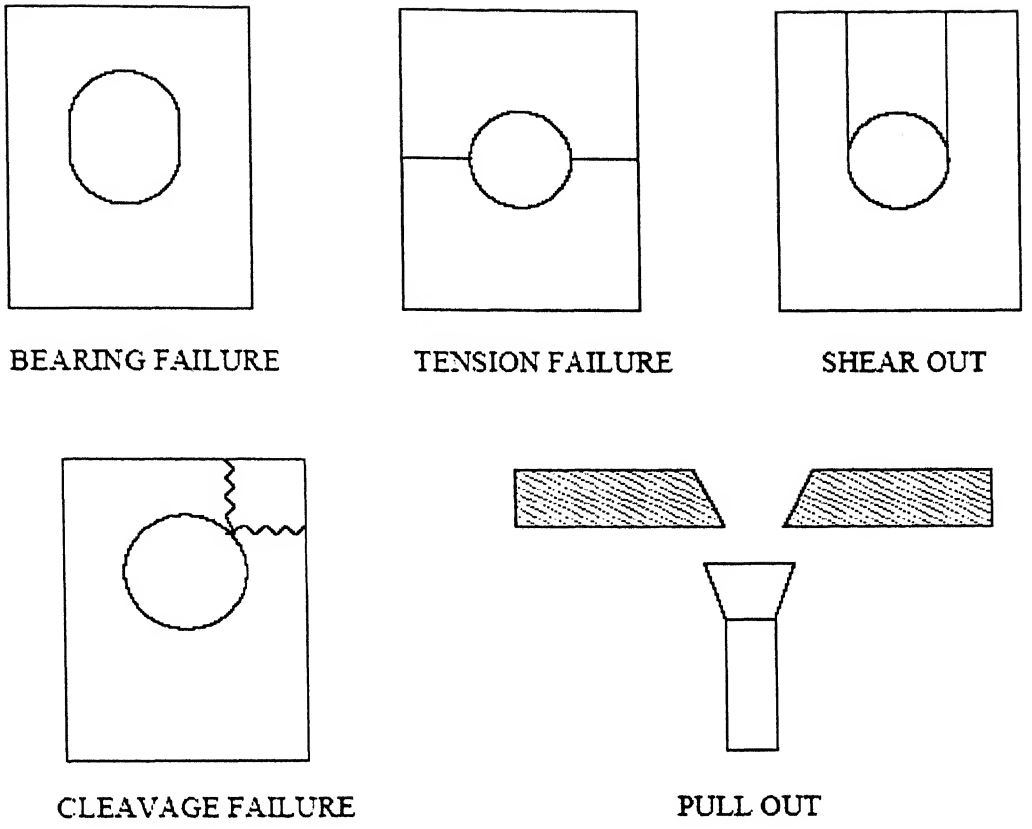

Figure 1.1: Failure modes of composite material

Figure 1.1 explains the first five modes of failures. These are common failure modes for isotropic material as well as the composites or orthotropic materials. Composite materials show an extra mode of failure called delamination. It is considered to be of prime importance and researchers are still pondering on this failure mode.

While making holes by drilling process, fiber debonding and ply separation are likely to occur. Fiber debonding leads to a crack in a lamina which can be developed into an inter-facial crack. Ply separation further leads to the inter-facial or inter-laminar crack, commonly referred as delamination. Thus, delamination generally starts at the hole boundary. In practice delamination can start from free surface, loaded surface or from foreign material or due to matrix decohesion.

Delamination has distinguished effects on stress concentration near hole boundaries. It normally leads to stress relaxation and hence alters the stress distribution near hole boundary. Once delamination is initiated or in fracture

mechanics terms, nucleated, it propagates along the interface to result in complete ply separation. Due to ply separations each ply bears the load individually. Naturally, this result into low load bearing capacity, compared to the composite laminate without flaw. This individuality accelerates the failure process and may lead to catastrophic failure. Hence this thesis is devoted to investigate delamination initiation and propagation.

Delamination can be viewed as inter-facial crack, and hence, fracture mechanics concepts can be applied to investigate delamination. For this purpose cohesive zone theory is used to model delamination, as it has specific advantages over conventional fracture mechanics methods such as LEFM, elasto-plastic, or J-integral method. It should be noted that the cohesive zone models are nonlinear in nature and hence nonlinearity is introduced into the problem.

1.2 Literature Review

Though considerable amount of work has been done to study the fracture phenomena through numerical methods, only rectangular beam (DCB) specimens were given special interest. Owen and Shantaram [26] started the case of finite element method to study dynamic crack growth. They studied DCB specimen and pipeline problem under transient loading.

Nishioka and Atluri [27] investigated the crack propagation and arrest in high strength steel DCB specimen using moving singular dynamic finite element procedure. An edge crack in a rectangular DCB specimen was propagated by inserting a wedge and the results were compared with experimental data. In another work, Nishioka and Atluri [28] presented the results of generation and prediction studies of dynamic crack propagation in plane stress and plane strain cases. The studies were conducted by using FEM, taking into account stress singularity near the crack tip. Variation of dynamic stress intensity factor with time and variation of dynamic fracture toughness with velocity were studied and compared with available experimental results.

For solving the crack problem cohesive zone model was used by many researchers. The cohesive zone idea was originally proposed by Barrenblatt [4] proposed

Cohesive zone model as a possible alternative to the concepts of fracture mechanics in perfectly brittle materials.

Dugdale [5] extended the concept of cohesive zone theory to perfectly plastic materials, by postulating the existence of a process zone at the crack tip. Dugdale applied the cohesive zone model to predict yielding of thin ideal elastic- plastic thin sheets containing slits.

Needleman [6,7] was one of the first to propose polynomial and exponential based traction-separation laws for Cohesive zone model. Needleman analyzed a range of problems using Cohesive zone model, some of them were, particle debonding in metal matrix [6], tensile decohesion along an interface [7,8,9].

Xu and Needleman [10] further used the above models to study the void nucleation at interface between particle and matrix.

Tvergaard [11], developed a similar model to that of Needleman. The formulations were identical for purely normal separation but Tvergaard coupled normal and tangential displacements to predict coexistence of three modes of crack. He modeled the decohesion of transversely staggered SiC whiskers in an aluminium matrix and subsequent void formation by normal and tangential separation. He also investigated fibre fracture and decohesion for a similar system with transversely aligned fibres.

Tvergaard and Hutchinson [12] forwarded a bilinear type of cohesive zone model and showed relation between crack resistance curve and fracture process parameters.

Li and Chandra [13] were the first to show the effect of form/shape of cohesive zone model in predicting the crack growth resistance and the size of plastic zone surrounding the crack tip, besides the effect of material parameters. They found that in addition to cohesive strength and cohesive energy, the form/shape of traction separation law of cohesive zone model plays a critical role in determining the crack growth resistance which clearly contradicts with the then common belief about the superfluousness of the shape. Chandra et al [14] showed the form dependency by evaluating the response in titanium matrix composites reinforced by silicon carbide fibres with two different forms (bilinear and exponential) of Cohesive zone model.

EI Sayed and Sridharan [15] used Cohesive zone model to analyze two cases viz., a DCB specimen and a compressed composite beam. They proposed to work in terms of stresses and strains of the material of cohesive layer instead of traction and

displacement jumps. They employed a model proposed by Needleman [6] with a failure criterion based on the energy release rates in different modes.

1.3 Overview of the work

As mentioned in the previous sections, that delamination is the one of the important failure modes present in the mechanically fastened joints. Simulation of the delamination initiation and propagation is attempted in this work. Delamination is considered as an interface crack. Cohesive zone model is used to simulate this crack.

For modeling the cohesive zone, special type of elements called cohesive elements are formulated. The cohesive elements are the four-node elements with zero area. A two dimensional plain strain formulation is adopted for the calculating stiffness and forces for the cohesive element.

The composite material is assumed to bear a linear stress strain relationship. The composite laminae are modeled using the four noded isoparametric element. The quadratic cohesive zone model is used as the cohesive zone's governing traction displacement law. This cohesive zone's constitutive equations introduce a material nonlinearity into the problem.

The two dimensional plain strain formulation is adopted to simulate the crack propagation in DCB specimen. A hypothetical problem is considered for steel specimen in which dynamic force pulse is applied at the top of the specimen. Variations of energy release rate with various other parameters are studied. Along with these, experimental input data (Chowdhary [25]) are used to simulate crack propagation in graphite/epoxy DCB specimen.

1.4 Thesis Organization

The thesis report is presented in five chapters, as follows:

Chapter2 discusses the various processes involved in the process zone and the cohesive zone model which is to be used during the analysis.

Chapter3 describes the basics of two dimensional plain strain formulation for the composite material and the cohesive zone. It also describes the calculation of energy release rates.

Chapter4 describes the results and discussion.

Chapter5 describes the conclusion of the present work and the scope of future work.

Chapter 2

Theory of Cohesive Zone and Failure Criterion

In this Chapter a brief discussion of various energies involved in cohesive zone and the model are presented.

2.1 Introduction

Conventional fracture mechanics, like linear elastic fracture mechanics, uses some idealized conditions which deviate from real situations. These theories characterize the crack by using single parameters such as stress intensity factors or energy release rates. These theories suffer from a disadvantage that near crack tip the stresses are singular, which is practically unrealistic. They assume the crack to be sharp, which may not always be the condition. The elastoplastic theory is somewhat generalized but it loses its usefulness when inelastic processes, such as plasticity, do occur near the crack tip, which are often observed in most of the materials.
While conventional methods fail to explain the fracture problem fully, cohesive zone theory is formed to model various intricacies involved. In the cohesive zone theory,

1. The stresses near the crack tip can be bounded.
2. Various inelastic, irreversible processes such as plasticity can be included.

3. Various dissipating mechanism active in fracture process zone can be captured and the contributions from the mechanisms can be delineated with fine spatial resolution.

2.2 Micro-mechanical aspects of the Cohesive Zone Model

A typical case of a crack in a body is shown in Figure 2.1. OA denotes the crack and A is crack tip. The cohesive zone is ahead of crack tip and is of length A. The estimate of cohesive zone length is given as (Freund [17]),

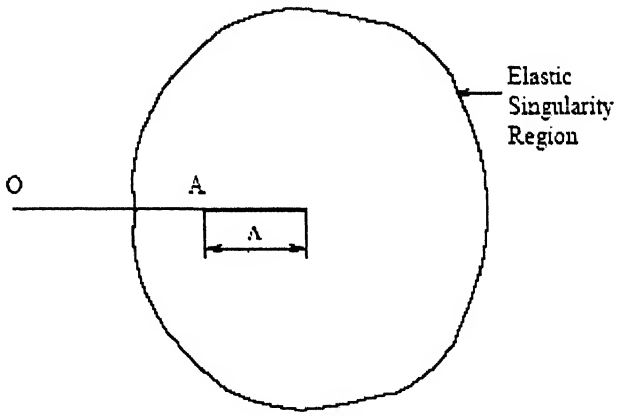

Figure 2.1: A crack in a body

$$\Lambda = \frac{\pi}{8}\left(\frac{K_{Iappl}}{\sigma_{max}}\right)^2 \qquad (2.1)$$

Where, σ_{max} is the maximum cohesive strength; K_{Iappl} is stress intensity factor due to applied load. Considering a region in the vicinity of the cohesive zone, shown in Figure 2.2, representing a crack tip process zone. Process zone can be defined as the region within the separating surfaces where surface traction values are nonzero. This clearly means that, processes occurring within the process zone are accounted through traction displacement law. In the most of cohesive zone models, the

traction separation relation for interfaces are such that, with increasing interface separation, the traction across the interface reaches a maximum then decreases and eventually vanishes, indicating complete decohesion.

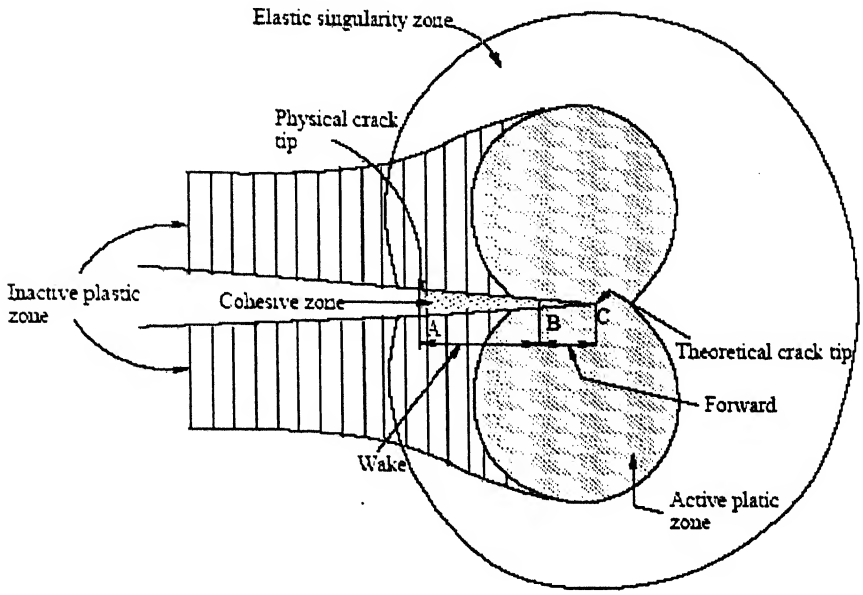

Figure 2.2: Crack tip with embedded process zone

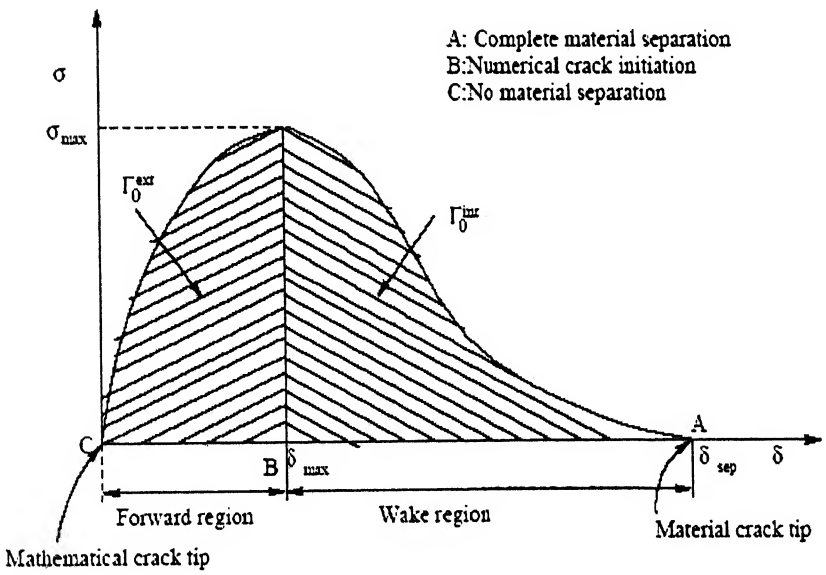

Figure 2.3: Typical traction separation curve of CZM and partition between intrinsic and extrinsic dissipation

For example consider a model shown in Figure 2.3.The significance of points A, B, C in Figure 2.2 and in Figure 2.3 is as follows:

Point A corresponds to maximum separation δ_{sep} which means that at point A the material is completely fractured and hence tractions are zero at that point. Thus, point A represents the actual crack tip, beyond which the material is fractured.

Point B corresponds to the maximum traction. The separation at this point is denoted as δ_{max}. Li and Chandra [13] called this point as a crack tip for representing the various quantities associated with the crack tip at this point. Point C corresponds to zero traction and zero separation. From this point theoretically the fracture surface starts to split. Hence, point C is usually referred as theoretical crack tip. Li and Chandra [13] referred the region stretching out from point B, i.e., peak cohesive stress to point C as forward region. The region stretching from peak stress, point B to point A is called as wake region

2.3 Inelastic processes in cohesive zone

During the fracture process, energy flows into the cohesive zone and region surrounding the cohesive zone. The rate, at which the inelastic processes develop within the cohesive zone, depends on the rates of dissipations caused by various mechanisms acting within the zone. Li and Chandra [13] has augmented that, since the energy flow is linked to micro-mechanics of fracture process, there should be a link between the active micro-mechanisms of a given material and that of traction-displacement curve.

Before going further, it is necessary to investigate the various processes in the following regions: the forward region of traction-displacement curve (Figure 2.3), where inelastic damage processes are occurring due to current loading conditions, and the wake region, where elastic unloading is taking place. The micro-structural damage mechanisms in forward region are called extrinsic dissipation, which generally promote the growth of crack, while dissipative mechanisms in wake region are called intrinsic dissipation. Generally, consumed energy in the intrinsic dissipation is partly distributed in boundary material and rest goes into crack/cohesive zone. Intrinsic dissipation depends on the length of newly formed

crack surfaces, while extrinsic dissipation is inherent property of material and doesn't depend upon geometric aspects.

Figure 2.4 shows the summery of many processes in the wake region and the forward region [13]. It can be noted that all the processes under intrinsic dissipation heading, such as crack deflection, crack closure, friction, etc., are dependent on crack surface length. All the processes, such as micro-cracking, void growth and coalescence in ductile fracture, phase transformations, which are included under the extrinsic dissipation heading, are material dependent.

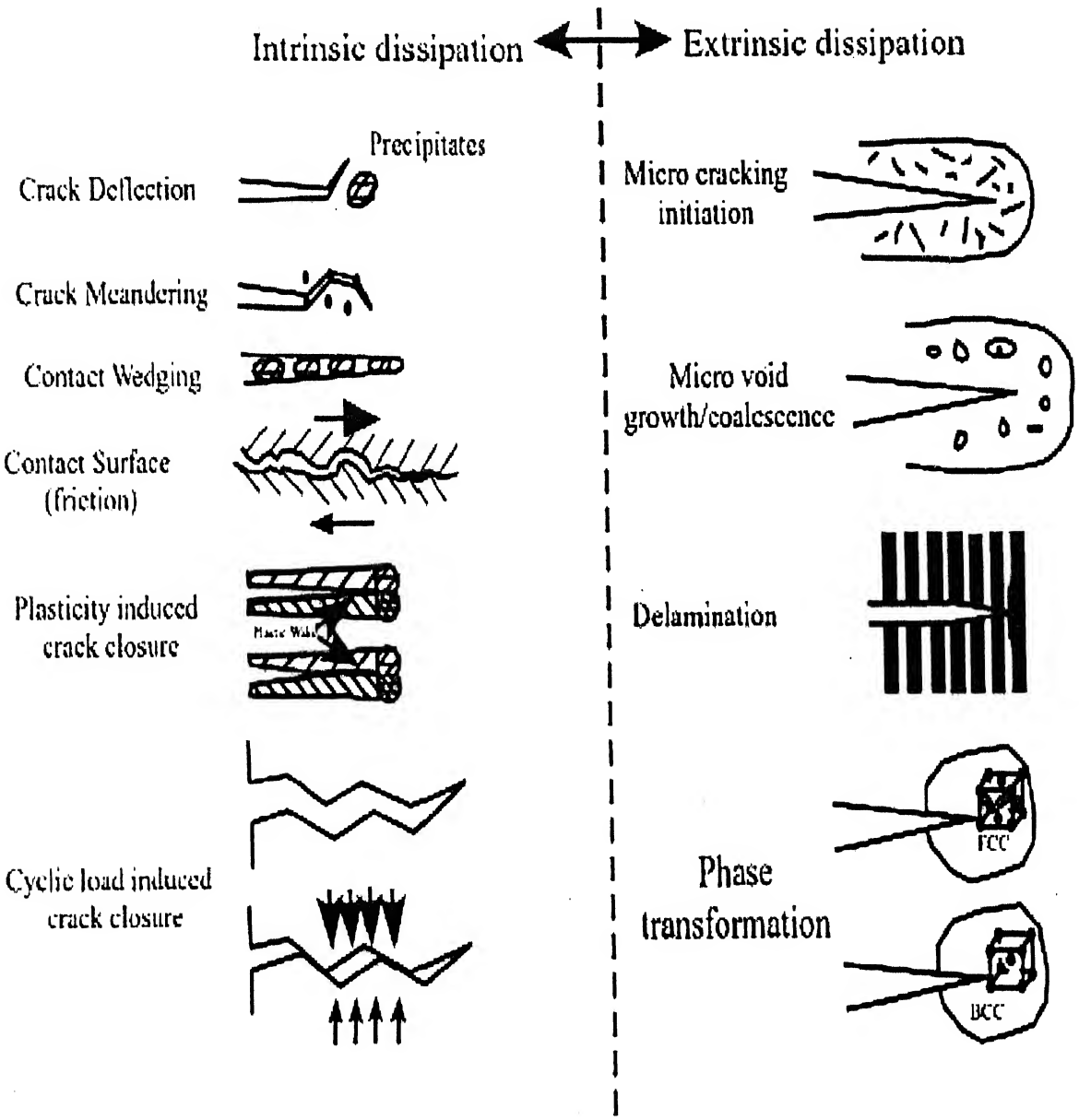

Figure 2.4: Energy dissipation mechanisms in the wake and forward regions [13].

2.4 Traction Separation law

The basic concept of cohesive zone is introduced by Barenblatt [4] for predicting material behavior near crack tip region. The idea is extend by Dugdale [5] for a thin steel slits problem. After that various traction-separation laws are put forward. A summery of the various proposed CZM along with their application (as used by the proposers), is given in a paper by Chandra et al [14], in a tabular form.

In the current analysis a cohesive zone model forwarded by Tvergaard [11] is used. Basically the model is postulated by Neddleman [8] and extended by Tvergaard [11]. The model used here is extrinsic type without rate dependency or history dependency. The cohesive zone model gives relation between tractions (T_n ; T_s) and displacements ([u_n] ; [u_s]) in local directions, n, s as follows,

$$T_n = \alpha_p \left(\frac{27}{4}\right) \sigma_{max} \left(\frac{[u_n]}{\delta_n}\right) \left(1 - 2\lambda + \lambda^2\right) \tag{2.2}$$

$$T_s = \alpha_s \left(\frac{27}{4}\right) \sigma_{max} \left(\frac{[u_s]}{\delta_s}\right) \left(1 - 2\lambda + \lambda^2\right) \tag{2.3}$$

where σ_{max} is a measure of bond strength in normal direction and is a material property, λ is a normalized quantity, i.e., $0 \leq \lambda \leq 1$ which couples normal and tangential behavior and is given by

$$\lambda = \sqrt{\left(\frac{[u_n]}{\delta_n}\right)^2 + \left(\frac{[u_s]}{\delta_s}\right)^2} \tag{2.4}$$

where, δ_n , δ_s are characteristic lengths in n, s directions, [u_n], [u_s] are the displacement jumps across the interface. In equations 2.3, 2.4, α_n, α_s are material parameters that help in defining the maximum traction in the respective directions. The maximum tractions in the n, s directions are σ_{max}, $\alpha_s \sigma_{max}$.

In pure normal separation ($[u_s] = 0$), the maximum traction is σ_{max}. Total separation occurs at $[u_n] = \delta_n$ and work of separation per unit interface area is given by

$$G_{IC} = \frac{9}{16}\sigma_{max}\,\delta_n \tag{2.5}$$

Similar analogies can be stated for pure shear out separation. Thus, the work of separation per unit interface area is given by,

$$G_{IIC} = \alpha_s \frac{9}{16}\sigma_{max}\,\delta_s \tag{2.6}$$

In common practice, choice of α_s, σ_{max} is made and the parameters δ_n, δ_s are chosen such that the energy release rates are matched. But it is a common belief that energy release rates are the most important parameters and other parameters have little effect on the fracture process (EI Sayed and Sridharan [15]).

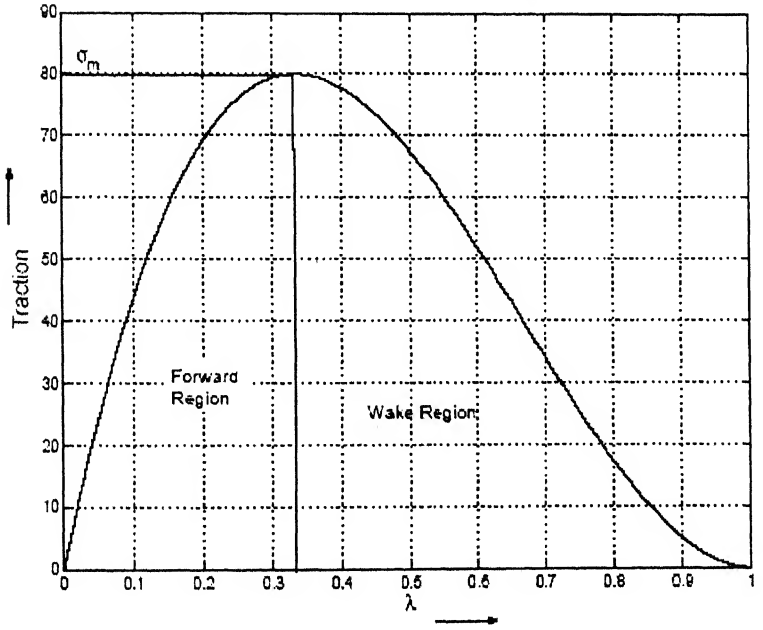

Figure 2.5: Normal Traction Separation Cohesive law

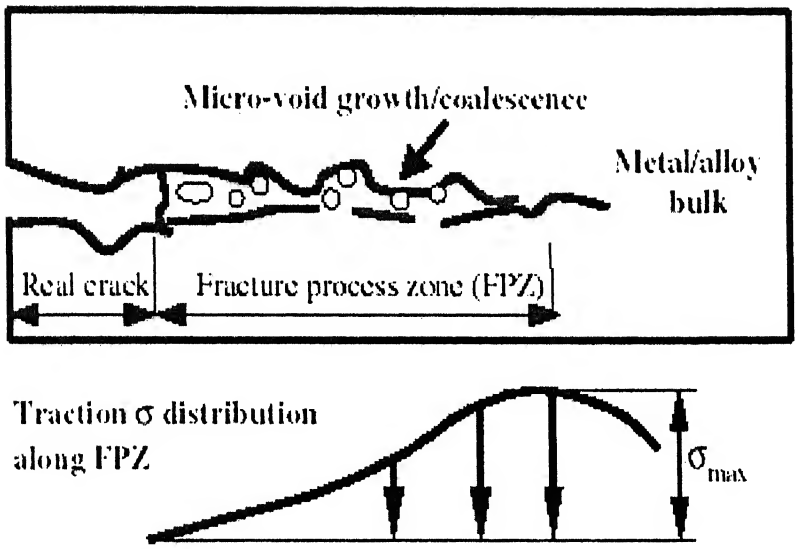

Figure 2.6: The tractions on the cohesive surfaces for normal separation

It should be noted that in the above cohesive zone model interaction of the different modes is achieved by a parameterλ. Displacement jump in any one direction results in change of traction values for all the three directions. The normal traction versus crack opening parameter for the normal separation is shown in Figure 2.5. In Figure 2.6 an elemental surfaces under normal mode of separation are shown. Here the n, s directions indicate local directions. Note that, all the above calculations are in local co-ordinate system.

The stiffness variation for a normal separation mode is shown in Figure 2.7. The stiffness terms will be derived later in the next Chapter. The stiffness decreases and becomes zero as $\lambda = 1/3$ is approached. Later it decreases to achieve a minimum (or maximum negative value) at point $\lambda = 2/3$. After this point, stiffness value increases and becomes zero at $\lambda = 1$. The positive stiffness corresponds to the extrinsic or forward region, while the negative stiffness corresponds to the intrinsic or wake region.

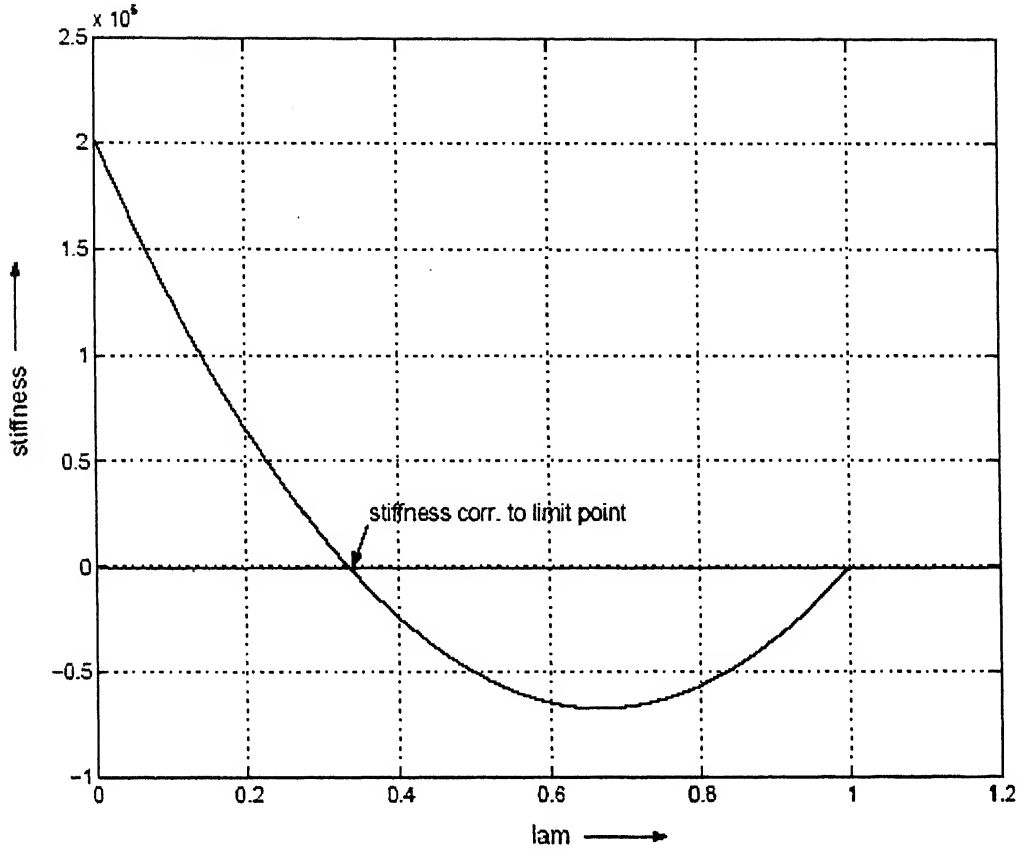

Fig 2.7: Stiffness versus Separation for normal separation

2.5 Failure criterion

In this Section a failure criterion for the cohesive zone model, described above, is discussed. As mentioned previously, the delamination is considered as the crack propagation problem. When the element fails, the crack is said to be propagated across the cohesive element. Two failure criteria are present in the literature. One of them is based on the energy consumed during the failure and its comparison with the energy release rates [15]. In the present analysis, a failure criteria based on the normalized parameter λ is employed. λ represents the normalized parameter, which

combines displacement jumps across the interface, for the three modes of crack, into a single quantity. The failure criterion is stated as follows: when λ reaches the value 1, the element is said to be failed. Thus, the cohesive element is capable of transferring the load when $0 < \lambda < 1$. But, when λ reaches the unity value, the tractions and stiffness at the gauss points are set to be equal to zero. Once the element has failed, the tractions and stiffness values are set to zero for further analysis.

Closure

In this chapter, a brief discussion of cohesive zone model is presented and the various inelastic processes occurring in the cohesive zone are summarized. In the next chapter the implantation are presented.

Chapter 3

Finite Element Formulation

3.1 Introduction

In this chapter a finite element formulation of cohesive zone model as applied to composite material is described. As the formulation for discretization of composite material can be found in many finite element text books, a very brief account of this is provided. However, a detailed description of finite element formulation of cohesive zone is provided.

3.2 FEM formulation

Equations that govern the dynamic response of a structural are derived by using virtual work principle involving work of external forces, internal, inertial and viscous forces for any small admissible motions.

The finite element solution involves discretization of domain (Ω) into suitable elements and approximating the field variable interior to the element in terms of nodal values using suitable shape function.

FEM equation can be derived from the virtual equation for the body as

$$\int_{\Omega}\{\delta\varepsilon\}^{T}\{\sigma\}dV+\int_{\Omega}\{\delta q\}^{T}\rho\{\ddot{q}\}dV+\int_{\Omega}\{\delta q\}^{T}k_{d}\{\dot{q}\}dV$$

$$=\int_{\Omega}\{\delta q\}^{T}\{P_{B}\}dV+\int_{\Gamma_{\sigma}}\{\delta q\}^{T}\{P_{s}\}dS \qquad (3.1)$$

where

$\{\delta q\}$, $\{\delta\varepsilon\}$: Virtual displacements and corresponding strains

$\{\dot{q}\}$, $\{\ddot{q}\}$: Velocity and acceleration component

$\{\sigma\}$: Stress component

ρ : Material density

k_d : Damping coefficient

$\{P_B\}$: Body forces

$\{P_S\}$: Surface traction

Γ_σ : Surface traction boundary

Displacements $\{q\}^{(e)}$ within element can be expressed in terms of its nodal values $\{Q\}^{(e)}$

As

$$\{q\}^{(e)}=[N]^{(e)}\{Q\}^{(e)} \qquad (3.2)$$

Strain-displacement relation can be written as

$$\{\varepsilon\}^{(e)}=[B]^{(e)}\{Q\}^{(e)} \qquad (3.3)$$

Stress-strain relation or constitutive equation is given as

$$\{\sigma\}^{(e)}=[D]^{(e)}\{\varepsilon\}^{(e)}=[D]^{(e)}[B]^{(e)}\{Q\}^{(e)} \qquad (3.4)$$

where

$[N]^{(e)}$ - Matrix of shape function

$[B]^{(e)}$ – Strain displacement matrix

$[D]^{(e)}$ – Matrix of material properties

The present analysis is made for an undamped system and neglecting body forces. The stresses, strains and displacements are expressed in terms of nodal variables as given in equations 3.2, 3.3 and 3.4. This on substitution in Eqn (3.1) gives,

$$\left[\sum_{e=1}^{N_E}\left(\int_{\Omega^{(e)}}[B]^{(e)^T}[D]^{(e)}[B]^{(e)}\,dv\right)\{q\}+\sum_{e=1}^{N_E}\left(\int_{\Omega^{(e)}}\left(\rho[N]^{(e)^T}[N]^{(e)}\,dv\right)\right)\{\ddot{q}\}-\sum_{e=1}^{N_E}\left(\int_{T_\sigma^{(e)}}[N]^{(e)^T}[P_s]^{(e)}\,ds\right)\right]\{\delta q\}^T=0 \tag{3.5}$$

where summation is over all elements, N_E.

since $\{\delta q\}$ is taken arbitrary, satisfying kinematic conditions, the equation can be written as,

$$\sum_{e=1}^{N_E}\left(\int_{\Omega^{(e)}}[B]^{(e)^T}[D]^{(e)}[B]^{(e)}|J|d\eta d\xi\right)\{q\}+\sum_{e=1}^{N_E}\left(\int_{\Omega^{(e)}}\rho[N]^{(e)^T}[N]^{(e)}|J|d\eta d\xi\right)\{\ddot{q}\}=\sum_{e=1}^{N_E}\left(\int_{T_\sigma^{(e)}}[N]^{(e)^T}[P_s]^{(e)}|J|d\eta d\xi\right) \tag{3.6}$$

The final set of assembled equations can be written as,

$$[K]\{Q\}+[M]\{\ddot{Q}\}=\{F\} \tag{3.7}$$

where

$[M] = \sum [M]^{(e)}$, Global mass matrix

$[K] = \sum [K]^{(e)}$, Global stiffness matrix

$\{F\} = \sum \{F\}^{(e)}$, Global applied force vector

and

$$[K]^{(e)} = \int_{\Omega^{(e)}}[B]^{(e)^T}[D]^{(e)}[B]^{(e)}|J|d\xi d\eta \quad \text{, Elemental stiffness matrix}$$

$$[M]^{(e)} = \int_{\Omega^{(e)}}\rho[N]^{(e)^T}[N]^{(e)}|J|d\xi d\eta \quad \text{, Elemental mass matrix} \tag{3.8}$$

$$\{F\}^{(e)} = \int_{\Gamma^{(e)}}[N]^{(e)^T}\{P_s\}^e|J|d\xi \quad \text{, Elemental force vector}$$

3.3 Finite Element formulation for cohesive element

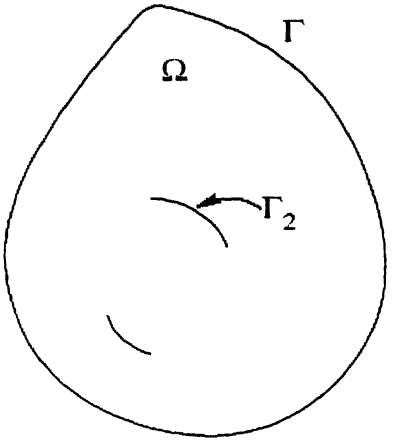

Figure 3.1: General domain with fixed external and time dependent internal boundary

Considering a boundary value problem, as shown in Figure 3.1. A domain Ω with boundary Γ has a time dependent boundaries (may be formed by the crack surface) Γ_I. Γ_I is viewed as an *internal time dependent boundary*. The following briefly gives the details of the FE modeling.

For a no body force condition, the principle of conservation of momentum is given by

$$\sigma_{ij,j} = 0.$$

If σ_{ij} is *statically admissible* stress field and δu_i is *kinematiclly admissible displacement field,* then principle of minimum potential energy leads to the equation,

$$\int_{\Omega} \sigma_{ij,j} \delta u_i \, d\Omega = 0 \tag{3.9}$$

where, δu_i are virtual displacements. It is to be noted that, in deriving above equation, a multiplication of displacement field δu_i with momentum conservation equation and symmetry of σ_{ij}, is used. Also in this formulation, use of the total Lagrangian formulation with infinitesimal strain measure is made.

Applying divergence theorem to equation 3.9, the left hand side will yield,

$$\int_{\Omega} \sigma_{ij,J}\,\delta u_i\, d\Omega = \int_{\Omega} \sigma_{ijJ}\,\delta u_{i,j}\, d\Omega - \int_{(\Gamma+\Gamma_2(t))} \sigma_{ij} n_j\,\delta u_i\, d(\Gamma+\Gamma_2)$$

$$= \int_{\Omega} \sigma_{ijJ}\,\delta \varepsilon_{i,j}\, d\Omega - \int_{(\Gamma+\Gamma_2(t))} T_i u_i\,\delta u_i\, d(\Gamma+\Gamma_2) \qquad (3.10)$$

Equation 3.10 along with equation 3.9 results in the equation,

$$\int_{\Omega} \sigma_{ij}\,\delta\varepsilon_{ij}\, d\Omega = \int_{\Gamma} T_i\,\delta u_i\, d\Gamma + \int_{\Gamma_2(t)} T_i\,\delta u_i\, d\Gamma_2$$

the various terms in the above equation show time dependence due to load nature and time dependence of internal boundary. Let the equilibrium state at time t + Δt is to be sought. Then, writing explicit time dependence of various terms in above equation, leads to

$$\int_{\Omega} \sigma_{ij}(t+\Delta t)\,\delta\varepsilon_{ij}(t+\Delta t)\, d\Omega = \int_{\Gamma} T_i(t+\Delta t)\,\delta u_i(t+\Delta t)\, d\Gamma + \int_{\Gamma_2(t)} T_i(t+\Delta t)\,\delta u_i(t+\Delta t)\, d\Gamma_2 \qquad (3.11)$$

The incremental values for each parameters involved in the above equation are defined as follows,

$$\Delta T_i = T_i(t+\Delta t) - T(t)$$

$$\Delta u_i = u_i(t+\Delta t) - u_i(t)$$

$$\Delta \sigma_{ij} = \sigma_{ij}(t+\Delta t) - \sigma_{ij}(t)$$

$$\Delta \varepsilon_{ij} = \varepsilon_{ij}(t+\Delta t) - \varepsilon_{ij}(t)$$

Substituting above deflections of incremental forms in equation 3.11, the following equation is obtained:

$$\int_{\Omega}\left[\left(\sigma_{ij}(t)+\Delta\sigma_{ij}\right)\delta\varepsilon_{ij}(t)+\sigma_{ij}(t)\delta\Delta\varepsilon_{ij}\right]d\Omega+\int_{\Omega}\Delta\sigma_{ij}\delta\Delta\varepsilon_{ij}d\Omega$$
$$=\int_{\Gamma}\left[T_i(t+\Delta t)\delta u_i(t)+T_i(t)\delta\Delta u_i+\Delta T_i\delta\Delta u_i\right]d\Gamma+$$
$$\int_{\Gamma_{2(t)}}\left[T_i(t+\Delta t)\delta u_i(t)+T_i(t)\delta\Delta u_i+\Delta T_i\delta\Delta u_i\right]d\Gamma_2$$

Considering changes in variational displacement field and traction to be small for a small time step Δt and neglecting their product term, the above equation can be restated as,

$$\int_{\Omega}\sigma_{ij}(t)\delta\Delta\varepsilon_{ij}d\Omega+\int_{\Omega}\Delta\sigma_{ij}\delta\Delta\varepsilon_{ij}d\Omega=\int_{\Gamma}\left(T(t)+\Delta T_i\right)d\Gamma+\int_{\Gamma_2(t)}\left(T_i(t)+\Delta T_i\right)d\Gamma_2$$

. (3.12)

Equation 3.12 represents the virtual work for a general body with initial and time dependent boundaries.

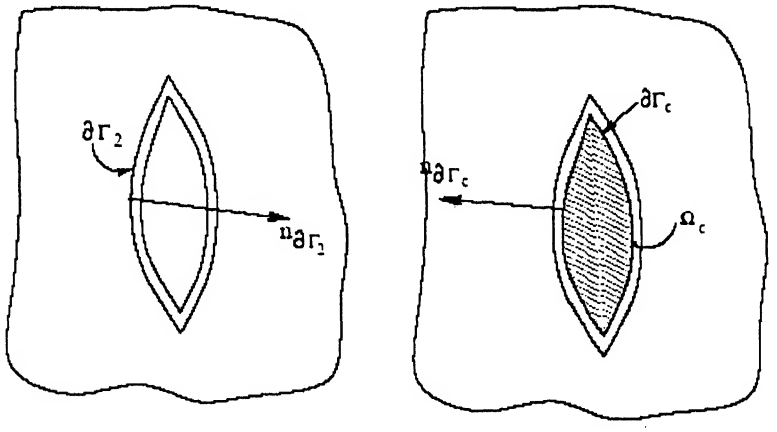

Figure 3.2: Cohesive zone included between internal time dependent boundaries

Having derived the virtual work expression in a general sense, focus is turned on the cohesive zone. Figure 3.2 shows a magnified view of the cohesive zone. In Figure 3.2, $\partial\Gamma_2(t)$ represents the boundary of fracture zone on domain side with $n_{\partial\Gamma_2}$ representing the normal to this boundary. $\partial\Gamma_c(t)$ represents the boundary of

cohesive zone with $n_{\partial\Gamma_c}$ representing the normal to this boundary. These boundaries are shown separately in Figure 3.2. It is clear from Figure 3.2 that the normals should be in opposite directions. Hence

$$n_{\partial\Gamma_2}(t) = -n_{\partial\Gamma_c}(t)$$

and

$$\partial\Gamma_2(t) = \partial\Gamma_c(t)$$

considering the above relations, the relation between the tractions acting on the two surfaces can be stated as,

$$T_i\left(n_{\partial\Gamma_2}(t)\right) = -T_i\left(n_{\partial\Gamma_c}(t)\right) \tag{3.13}$$

Making use of equation 3.13, equation 3.14 can be restated for a virtual work of cohesive zone as,

$$\int_{\Gamma_c}\Delta T_i\delta\Delta u_i\,d\Gamma_c + \int_{\Omega}\Delta\sigma_{ij}\delta\Delta\varepsilon_{ij}\,d\Omega_c = -\int_{\Gamma_c}T_i(t)\delta\Delta u_i\,d\Gamma_c - \int_{\Omega_c}\sigma_{ij}(t)\delta\Delta\varepsilon_{ij}\,d\Omega \tag{3.14}$$

At this stage it is assumed that, in initial configuration, the cohesive zone has no volume and hence, completely described by the boundaries and the tractions applied on them. Hence at any arbitrary time t, the incremental form of equation 3.14 reduces to

$$\int_{\Gamma_c(t)}\Delta T_i\delta\Delta u_i\,d\Gamma_c = -\int_{\Gamma_c}T_i(t)\delta\Delta u_i\,d\Gamma_c \tag{3.15}$$

With the aid of tangent stiffnesses, the incremental form of the tractions can be written as,

$$\Delta T_i = k_{ij}\Delta[u_j] + \Delta T_i^R \tag{3.16}$$

The second term in the equation 3.16 takes care of rate dependent traction separation law. If the rate dependency is neglected, as specified in the previous Chapter, the equation becomes,

$$\Delta T_i = k_{ij} \Delta [u_j] \tag{3.17}$$

The k_{ij} terms in the above equation are obtained by differentiating equations 2.3, 3.4 with respect to displacement jumps $[u_j]$ i.e. $k_{ij} = \partial T_i / \partial [u_j]$. Hence for respective local n, s directions, k_{ij} are given as,

$$k_n = \left(\frac{27}{4}\right)\frac{\sigma_{max}}{\delta_n}\left[\left(1-2\lambda+\lambda^2\right)+\frac{1}{\lambda}\left(\frac{[u_n]}{\delta_n}\right)^2\left(-2+2\lambda\right)\right] \tag{3.18}$$

$$k_s = \alpha_s\left(\frac{27}{4}\right)\frac{\sigma_{max}}{\delta_s}\left[\left(1-2\lambda+\lambda^2\right)+\frac{1}{\lambda}\left(\frac{[u_n]}{\delta_s}\right)^2\left(-2+2\lambda\right)\right] \tag{3.19}$$

Note that above relations are valid for rate independent traction-displacement law. The variation of k_n with separation parameter λ was given in a Figure 2.7.
Substituting equation 3.16 into equation 3.14 the variational form is obtained as,

$$\int_{\Gamma_c(t)} k_{ij}\Delta[u_j]\delta\Delta u_i d\Gamma_c = -\int_{\Gamma_c(t)} T_i(t)\delta\Delta u_i d\Gamma_c \tag{3.20}$$

For simplicity, surface of cohesive zone is divided into two parts, viz. upper surface and lower line. So, the total boundary at any time is viewed as an addition of these two lines. We can write explicitly, what it means, in terms of equation as,

$$\Gamma_c(t) = \Gamma_c^l(t)$$

where, letters u and l, denote the quantities related to upper line and lower line respectively.

Rewriting the incremental variational form of equation 3.20 in terms of upper line and lower line, the virtual work equation for a cohesive zone is obtained as,

$$\int_{\Gamma_c^u(t)} k_{ij}\Delta[u_j]\delta\Delta u_i d\Gamma_c^u + \int_{\Gamma_c^l(t)} k_{ij}\Delta[u_j]\delta\Delta u_i d\Gamma_c^l$$

$$= -\int_{\Gamma_c^u(t)} T_i(t)\delta\Delta u_i d\Gamma_c^u - \int_{\Gamma_c^l(t)} T_i(t)\delta\Delta u_i d\Gamma_c^l \qquad (3.21)$$

3.3.1 Finite Element Discretization

The cohesive surface is discretized using a four-node zero area 2-D rectangular elements. These elements are generally called as cohesive elements. Thus, the discretization of equation 3.21 in space is carried out by stating displacement field, on each surface, as a function of nodal displacements.

Nodal displacements on upper and lower lines are indicated by $u_i^\alpha(u)$ and $u_i^\alpha(l)$ respectively, where u and l denotes the upper line and lower line respectively, superscript α denotes the node number and subscript i denotes the direction (n, s). Thus for an element shown in Fig 3.3, one has $\alpha \in (1; 2)$ and $i \in (1; 2)$.

Next, the assumptions for the upper and lower lines are stated clearly and separately as,

The upper line:

$$u_i = N^\alpha u_i^\alpha(u) \quad \text{and} \quad \Delta u_i = N^\alpha u_i^\alpha(u)$$

The lower line:

$$u_i = N^\alpha u_i^\alpha(l) \quad \text{and} \quad \Delta u_i = N^\alpha u_i^\alpha(l)$$

Where, N^α denote the interpolation functions or shape functions. With the help of above assumptions the displacement jumps, for the upper and lower lines, are given as,

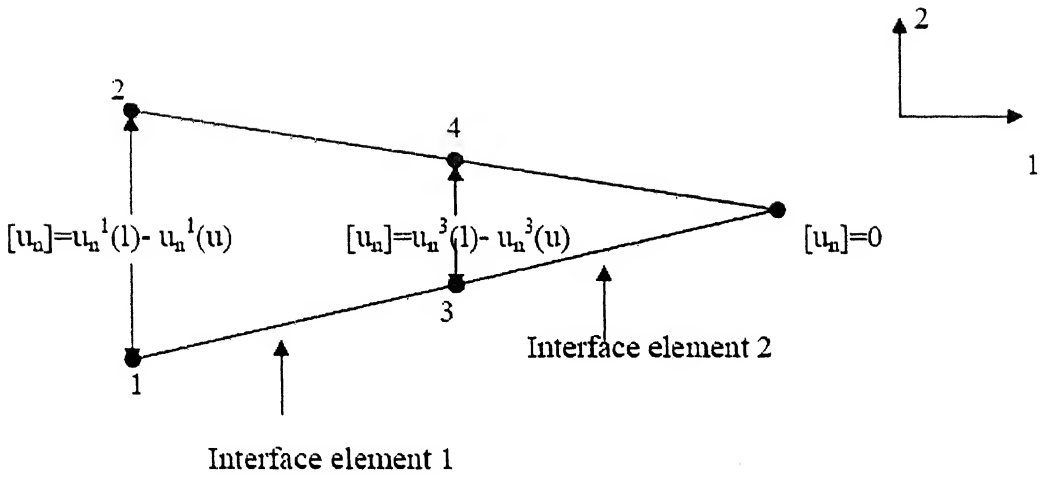

Figure 3.3: Crack opening displacement in mode I for a linear interpolated displacement field

Upper Line:

$$[u_i] = u_i(u) - u_i(l) = N^\alpha u_i^\alpha(u) - N^\alpha u_i^\alpha(l)$$

$$\Delta[u_i] = \Delta u_i(u) - \Delta u_i(l) = N^\alpha \Delta u_i^\alpha(u) - N^\alpha \Delta u_i^\alpha(l)$$

Lower Line:

$$[u_i] = u_i(l) - u_i(u) = N^\alpha u_i^\alpha(l) - N^\alpha u_i^\alpha(u)$$

$$\Delta[u_i] = \Delta u_i(l) - \Delta u_i(u) = N^\alpha \Delta u_i^\alpha(l) - N^\alpha \Delta u_i^\alpha(u)$$

Using the above assumptions, the equation 3.21 is rewritten as,

$$\int_{\Gamma_c^u(t)} k_{ij}\left[N^\beta \Delta u_j^\beta(u) - N^\beta \Delta u_j^\beta(l)\right] N^\alpha \delta\Delta u_j^\alpha(u)\, d\Gamma_c^u(t) +$$

$$\int_{\Gamma_c^l(t)} k_{ij}\left[N^\beta \Delta u_j^\beta(l) - N^\beta \Delta u_j^\beta(u)\right] N^\alpha \delta\Delta u_j^\alpha(u)\, d\Gamma_c^l(t)$$

$$= -\int_{\Gamma_c^u} T_i(t) N^\alpha \delta\Delta u_j^\alpha(u)\, d\Gamma_c^u(t) - \int_{\Gamma_c^l} T_i(t) N^\alpha \delta\Delta u_j^\alpha(l)\, d\Gamma_c^l(t) \quad (3.22)$$

Assuming linear variation of displacement field on upper line as well as on lower line, the shape functions are defined as,

$$N^{\alpha} = (1/2)(1+\xi_0)$$

where, $\xi_0 = \xi\xi^{\alpha}$ and ξ^{α} take values +1 or -1 depending upon the local coordinates of nodes. $\alpha \in (1; 2)$ corresponds to the node number. Same shape functions are assumed for upper as well as lower line.

Factoring out the virtual displacements and separating out the equilibrium equations for upper and lower lines, two equations are obtained as,

$$\int_{\Gamma_c^u(t)} k_{ij} N^{\alpha} N^{\beta} \left[\Delta u_j^{\beta}(u) - \Delta u_j^{\beta}(l)\right] d\Gamma_c^u(t) = -\int_{\Gamma_c^u(t)} T_i(t) N^{\alpha} d\Gamma_c^u(t)$$

$$\int_{\Gamma_c^l(t)} k_{ij} N^{\alpha} N^{\beta} \left[\Delta u_j^{\beta}(l) - \Delta u_j^{\beta}(l)\right] d\Gamma_c^l(t) = -\int_{\Gamma_c^l(t)} T_i(t) N^{\alpha} d\Gamma_c^l(t)$$

Above equations can be written in matrix form as,

$$K_{ij}(u)\left\{\Delta u_j^{\beta}(u) - \Delta u_j^{\beta}(l)\right\} = F_i(u)$$

$$K_{ij}(l)\left\{\left\{\Delta u_j^{\beta}(l)\right\} - \Delta u_j^{\beta}(u)\right\} = F_i(l)$$

The above matrix equations can be rewritten as,

$$\begin{bmatrix} K_{ij}(l) & -K_{ij}(l) \\ -K_{ij}(u) & K_{ij}(u) \end{bmatrix} \begin{Bmatrix} \Delta u_j^{\beta}(l) \\ \Delta u_j^{\beta}(u) \end{Bmatrix} = \begin{Bmatrix} F_i(l) \\ F_i(u) \end{Bmatrix} \tag{3.23}$$

where,

$$K_{ij}^{\alpha\beta}(l) = \int_{\Gamma_c^l(t)} k_{ij} N^{\alpha} N^{\beta} d\Gamma_c^l(t) \qquad K_{ij}^{\alpha\beta}(u) = \int_{\Gamma_c^l(t)} k_{ij} N^{\alpha} N^{\beta} d\Gamma_c^u(t)$$

$$F_i^{\alpha}(l) = -\int_{\Gamma_c^l(t)} T_i(t) N^{\alpha} d\Gamma_c^l(t) \qquad F_i^{\alpha}(u) = -\int_{\Gamma_c^l(t)} T_i(t) N^{\alpha} d\Gamma_c^u(t)$$

To make better understanding of above equations, explicit expressions for K_{ij} for directions n, s and for lower line are provided as follows,

$$K_p^{\alpha\beta}(l) = \int_{\Gamma_c^l(t)} k_p(l) N^\alpha N^\beta d\Gamma_c^l(t)$$

$$K_n^{\alpha\beta}(l) = \int_{\Gamma_c^l(t)} k_n(l) N^\alpha N^\beta d\Gamma_c^l(t)$$

$$K_s^{\alpha\beta}(l) = \int_{\Gamma_c^l(t)} k_s(l) N^\alpha N^\beta d\Gamma_c^l(t)$$

The remaining terms, like $K_{ps}^{\alpha\beta}, K_{pn}^{\alpha\beta}, K_{ns}^{\alpha\beta}$ are taken as null. $K_p^{\alpha\beta}, K_n^{\alpha\beta}, K_s^{\alpha\beta}$ may be derived for the upper and lower lines separately.

After substituting the expressions for K_{ij}, the general form of equation 4.16 becomes,

$$\begin{bmatrix} K_{lower} & -K_{lower} \\ -K_{upper} & K_{upper} \end{bmatrix} \begin{Bmatrix} \Delta u_{lower} \\ \Delta u_{upper} \end{Bmatrix} = \begin{Bmatrix} F_{lower} \\ F_{upper} \end{Bmatrix} \qquad (3.24)$$

where K_{lower} , K_{upper} and F_{lower} , F_{upper} represent assembled stiffness matrices and force vectors for the lower and upper line respectively. Δu_{lower}, Δu_{upper} are local incremental displacements vectors for lower and upper lines respectively. From the expressions in equation 3.24, it can be inferred that, basic differences for k_n, k_s for upper and lower lines come through difference between displacement jumps for the surfaces, as the shape functions are assumed to be same for the lines. But note that in the equations 3.18, 3.19 second power of displacement jumps are involved. Hence, essentially these terms are same for both the lines. Hence,

$$K_{upper} = K_{lower}$$

Scrutinizing the equations for the tractions in n, s directions (equations 2.3, 2.4) it can be stated that, tractions are exactly opposite to each other, as first power of displacement jumps are involved in their calculations. Hence it can be concluded that,

$$F_{upper} = -F_{lower}$$

Considering the relations between the stiffness matrices and force vectors for upper and lower lines, as inferred above, the equation 3.24 is simplified as,

$$\begin{bmatrix} K_{lower} & -K_{lower} \\ -K_{lower} & K_{lower} \end{bmatrix} \begin{Bmatrix} \Delta u_{lower} \\ \Delta u_{upper} \end{Bmatrix} = \begin{Bmatrix} F_{lower} \\ F_{lower} \end{Bmatrix} \qquad (3.25)$$

3.3.2 Global assembly

For an element shown in Figure 3.3, with linear variable displacement field i.e. $\alpha \in (1, 2)$, $K_{ij}(l)$ would be a 2 x 2 matrix. Thus two 2 x 2 matrices viz. $K_n(l)$, $K_s(l)$ are to be assembled to form a 4 x 4 matrix K_{lower}.

Similarly, force vector of size 4 x 1, assembled from 2 x 1 sized force vectors Fn, F_s.

Thus, from equation 3.25 cohesive element stiffness matrix is of 8 x 8 size and cohesive element force matrix is of 8 x 1 size.

Note that in the formulation, the local co-ordinate system is employed i.e. the displacement forms encountered are in local co-ordinate system. Before going for the calculations one has to transform the displacement vector in the global co-ordinate system, into the local one. Once the matrices and force vectors are formed using the local co-ordinate systems, then at the time of assembly they had to be transformed back in the global co-ordinate system. Mathematically this implies that,

$$K_{yz} = T^T K_{ns} T \qquad F_{yz} = T F_{ns}$$

Keeping the transformations in mind, we next move to global assembly of the cohesive element stiffness matrices and force vectors. It is interesting to know that, the global assembly of the matrices and vectors are simply carried out as, that for stiffness matrices and force vectors of any other usual finite element.

3.4.1 Integration Algorithms

Equations of equilibrium governing linear dynamic response of a system of finite element are given by Eqn (3.7).

Eqn 3.7 can be written as,

$$F_I(t) + F_E(t) = F(t) \tag{3.26}$$

where, $F_I(t)$ are inertia forces, $F_I(t) = [M]\{Q\}$, $F_E(t)$ are elastic forces, $F_E(t) = [K]\{Q\}$, all of them being time dependent. Thus, in dynamic analysis, the displacements $\{Q\}$, $\{\varepsilon\}$and $\{F\}$ are all functions of time.

Mathematically, for small deformation Δt can be assumed. Eqn (3.7) represent a system of linear differential equation of second order and the solution to the equation can be obtained by standard procedures of solving differential equations.

The procedures for solving differential equations are divided into direct integration and mode superposition of which former is preferred in wave propagation problem.

In this integration scheme, there are many different methods, which can be classified as 'Explicit' or 'Implicit' whose advantages and disadvantages are given by Bathe[29].

In the present work Newmark Integration scheme is used.

3.4.2 Newmark's Method of Integration

Newmark's method is an extension of 'Linear acceleration method', in which, linear variation of acceleration is assumed from time t to $t + \Delta t$.

Velocity and acceleration approximated in terms of displacements are

$$^{t+\Delta t}\{\dot{q}\} = {}^{t}\{\dot{q}\} + \left[(1-\delta)^{t}\{\ddot{q}\} + \delta^{t+\Delta t}\{\ddot{q}\}\right]\Delta t \tag{3.27}$$

$$^{t+\Delta t}\{q\} = {}^{t}\{q\} + {}^{t}\{\dot{q}\}\Delta t + \left[\left(\frac{1}{2}-\alpha\right)^{t}\{\ddot{q}\} + \delta^{t+\Delta t}\{\ddot{q}\}\right]\Delta t^2 \tag{3.28}$$

where α and δ are the parameters chosen suitably to have accuracy and stability. Usually, α and δ are taken as 0.25 and 0.5 respectively to get unconditional stability. As mentioned earlier, equilibrium at $t + \Delta t$ is considered along with these approximations. Solving equations 3.8 and 3.9, we get expressions for ${}^{t+\Delta t}\{\dot{q}\}$ and ${}^{t+\Delta t}\{\ddot{q}\}$, in terms of unknown displacements ${}^{t+\Delta t}\{q\}$.These are then substituted in the following equation to solve for ${}^{t+\Delta t}\{q\}$.

$$[M]^{t+\Delta t}\{\ddot{q}\}+[K]^{t+\Delta t}\{q\}={}^{t+\Delta t}\{F\} \tag{3.29}$$

Entire method can be summarised as follows

1. Form global stiffness matrix [K], and mass matrix [M].

2 Initialise ${}^{0}\{q\}, {}^{0}\{\dot{q}\}, {}^{0}\{\ddot{q}\}$.

3 Select time step Δt and calculate integration constants

$$a_0=\frac{1}{\alpha\Delta t^2}\ ;\ a_1=\frac{\delta}{\alpha\Delta t}\ ;\ a_2=\frac{1}{\alpha\Delta t}\ ;\ a_3=\frac{1}{2\alpha}-1 \tag{3.30}$$

$$a_4=\frac{\delta}{\alpha}-1\ ;\ a_5=\frac{\Delta t}{2}\left(\frac{\delta}{\alpha}-2\right)\ ;\ a_6=\Delta t(1-\delta)\ ;\ a_7=\delta\Delta t$$

For effective stiffness, $[K']=[K]+a_0[M]$ (3.31)

4 For each time step :

(i) Calculate effective load at $t+\Delta t$

$${}^{t+\Delta t}\{F'\}={}^{t+\Delta t}\{F\}+[M]\left(a_0^t\{q\}+a_2^t\{\dot{q}\}+a_3^t\{\ddot{q}\}\right) \tag{3.32}$$

(ii) Solve for displacement at time $t+\Delta t$ by $[K']^{t+\Delta t}\{q\}={}^{t+\Delta t}\{F'\}$ (3.33)

(iii) Calculate acceleration and velocity at time $t+\Delta t$

$${}^{t+\Delta t}\{\ddot{q}\}=a_0\left({}^{t+\Delta t}\{q\}-{}^{t}\{q\}\right)-a_2^t\{\dot{q}\}-a_3^t\{\ddot{q}\} \tag{3.34}$$

3.5 Energy Release Rate and its Determination

In fracture mechanics a crack can be characterized by four different parameters

a) Energy release rate (G_I G_{II} G_{III}) is energy based and is also applied to brittle and less ductile material.
b) Stress intensity factor (K_I , K_{II} , K_{III}) is stress based. This parameter is also applied to brittle and less ductile material.
c) J-Integral (J) which has been developed to deal with ductile material and can also be applied to brittle material as well.
d) Crack tip opening displacement (CTOD) is displacement based and is developed for ductile materials.

From computational point of view, stress intensity factor require special element so as to simulate stress singularity at the crack tip whereas J-Integral and energy release do not require any such modeling of stress singularity. In energy release rate approach, energy is found out in entire domain and in J-Integral; evaluation is done along a path far away from crack tip. Thus both these approaches adroitly avoid analysis close to the crack tip and don't need any modeling of stress singularity.

Griffith [30] outlined that in brittle fracture, the extension of a crack requires the formation of new surface, he reasoned with its associated surface energy, consequently, crack in a brittle solid should advance when the reduction of the total potential energy of the body during a small amount of crack advance equals the surface energy of the new surface thereby created. Most of the energy release, as the crack advances, comes from the parts of the specimen which are adjacent to the cracked surface.

Two important parameters need to be considered

1) How much energy is released when a crack advance.
2) Minimum energy required for crack to advance in forming two mew surfaces.

First parameter is measured in terms of energy release rate denoted by G. G is a function of crack size in general. Energy release rate is the amount of energy

release per unit increase in area during crack growth. This energy is supplied by the elastic energy in the body and by the loading system.

The energy requirement for a crack to grow per unit area extension is called as crack resistance and is usually denoted by symbol R. Crack resistance is sum of energy required to 1) form new surface and 2) cause an elastic deformation.

Both the available energy release rate and crack resistance are important to study the possibility of crack becoming critical. Obviously, when the available energy release rate far exceeds the crack resistance, the crack starts to grow at high speed. In the present study 'energy release rate' is adopted as it is a more comprehensive concept.

As the crack advances,

1) Stiffness of the component decreases
2) Strain energy in the component either increases or decreases.
3) Work is done on the component if there is an application of load.
4) Energy is being consumed to create two new surfaces.

In the current analysis a cohesive zone model forwarded by Tvergaard [11] is used. Basically the model is postulated by Needleman [8] and extended by Tvergaard [11]. The model used here is extrinsic type without rate dependency or history dependency. The cohesive zone model gives relation between tractions (T_n) and displacements ($[u_n]$) in local direction 'n' as follows,

$$T_n = \left(\frac{27}{4}\right)\sigma_{\max}\left(\frac{[u_n]}{\delta_n}\right)\left(1-2\lambda+\lambda^2\right) \tag{3.36}$$

For a model where maximum cohesive strength σ_{max} and critical displacement δ are constants the amount of energy per unit area spent in the separation process , G, as described by this specific traction separation law is given by

$$G_{IC} = \frac{9}{16}\sigma_{\max}\,\delta_n \tag{3.37}$$

In common practice, choice of σ_{max} is made and the parameter δ_n are chosen such that the critical energy release rates are matched with the known data.
Energy release rate (G) is found by adding up the cohesive energy contributions from all N cohesive elements distributed in the finite element model Due to the use of variable σ_{max} and δ the cohesive energy spent in the N cohesive elements during crack growth has to be determined by integration

$$G = \sum_{i=1}^{N} \int (T_n) d(u_n)_i \qquad i=1, N \qquad (3.38)$$

During the crack propagation analysis energy release rate at each time step is calculated by the equation 3.38. For the first cohesive element failure the cohesive parameters are chosen such that the critical energy release rate values are matched with the experimental data. And for the other cohesive elements the values are chosen such that energy release rate varies smoothly.

3.6 Closure

In this chapter, formulation of FEM equation is described along with integration algorithms for solving equilibrium equation governing linear dynamic response of a system of finite element. This chapter also describes some general concepts in energy and energy release rate.

Chapter 4

Results And Discussion

4.1 Introduction

In this Chapter results of the dynamic crack propagation analysis are presented using the method described in the previous Chapters. First the method is validated for dynamic case. Later results are also presented for the available experimental data for crack propagation.

Various aspects of the results involve,

- Crack propagation under dynamic input force pulse.
- Crack propagation under time dependent input displacement (based on experimental data).

4.2 Test Problem

For the analysis purpose of investigating various aspects, a hypothetical problem of cantilever beam specimen is considered (Fig 4.1).In this test problem cohesive elements are inserted at the interface of the DCB specimen. The simulation is done for different combinations of cohesive zone materials parameters, viz., critical displacement jumps and maximum tractions for each element.

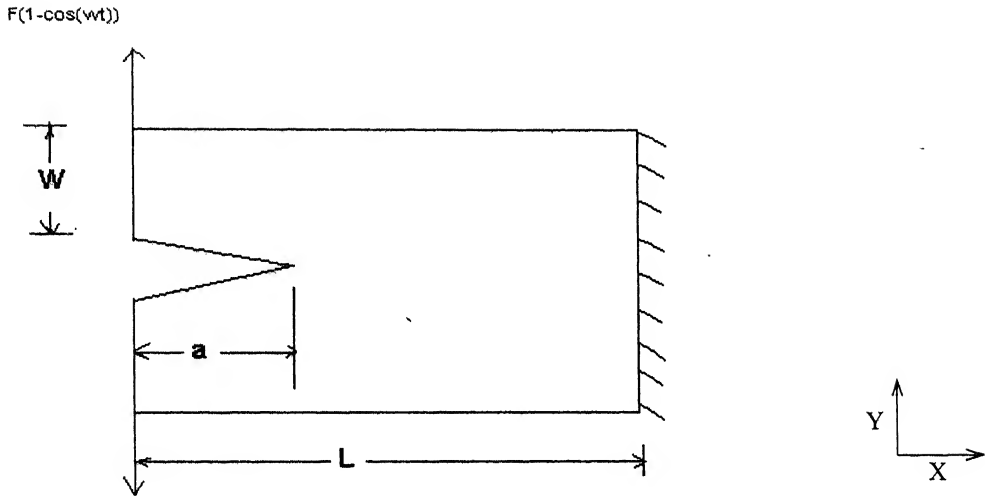

Fig 4.1 DCB Specimen

Material and geometric properties are as follows

- Modulus of Elasticity $E=210 \times 10^9$ N/m^2
- Poisson ratio $\upsilon = 0.3$
- Length of specimen L = 0.03 m
- Width of specimen W = 0.0025 m
- Thickness of specimen B = 0.012 m
- Crack length a = 0.015 m

The DCB specimen is analyzed by using four-noded isoparametric elements. Details are as follows

- Number of elements 120
- Number of nodes 124
- Size of element in X-direction 1.0 mm
- Size of element in Y-direction 1.25 mm

The cohesive elements are analyzed by four-noded linear elements. Details are as follows

- Number of cohesive elements 30
- Number of nodes 31
- Size of cohesive elements in X-direction 1.0 mm

For dynamic crack propagation, a short pulse is applied at the top of the specimen (Fig 4.2). The pulse can be modeled by F(1-cos(ωt)) whose details are as follows:

- Pulse duration $p = 52\ \mu s$
- Force amplitude $F_0 = 12\ N$
- Frequency of pulse $f = 19.23\ KHz$

Time step depends on the element size and wave velocity

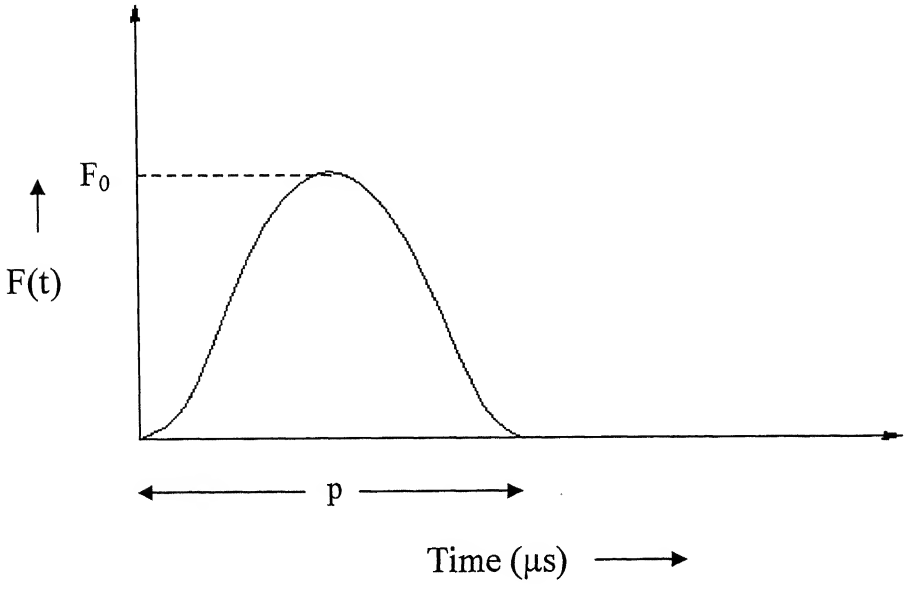

Fig 4.2 Input Force Pulse

Crack propagation starts after the force pulse of 52 μs is completely applied. Two different time steps are taken for the analysis

1) Before crack propagation $\Delta t_1 = 4.92 \times 10^{-6}$ sec

2) After crack propagation initiates Δt_2 = a reduced value for higher accuracy.

The meshing used for the DCB specimen is shown in Fig 4.3.

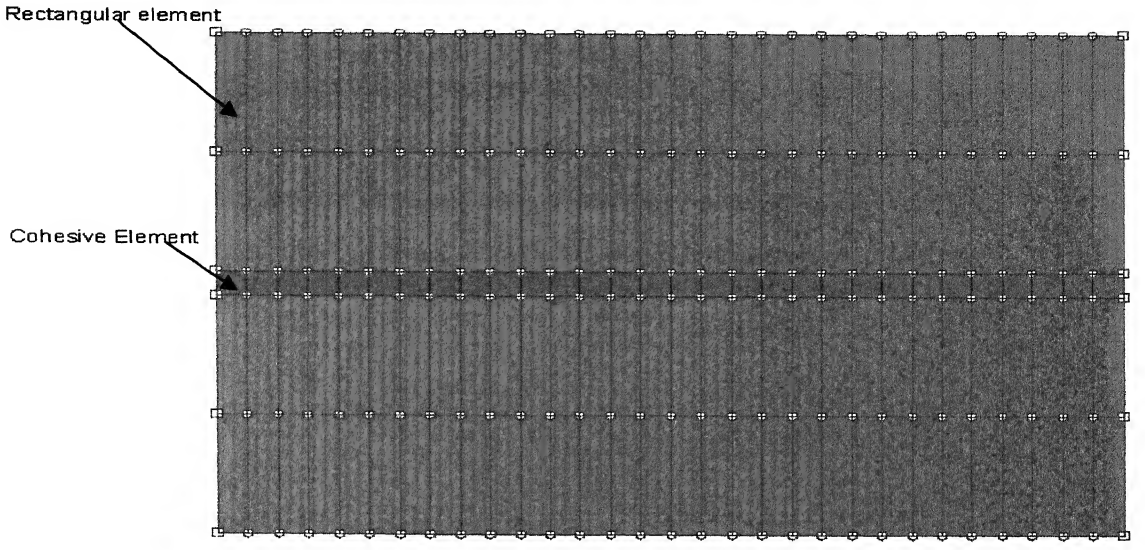

Fig 4.3 Meshing of DCB Specimen

The Table 4.1 lists different cases of cohesive element material properties studied. For the first cohesive element it is assumed that the critical energy release rates are

$G_{Ic} = 512$ J/m^2

$G_{IIc} = 904$ J/m^2

choice of α_s , σ_{max} is made and the parameters δ_n , δ_s are chosen such that the critical energy release rates are match well with the above mentioned values.

And for the other cohesive elements these parameters are chosen in such a way that the energy release rate for propagation decreases gradually. No effect of the change in α_s is observed , as expected, because this case represents pure mode I propagation.

Elements	σ_{max} (MPa)	δ_n (mm)	δ_s (mm)	α_s
First	130	0.007	0.0308	0.4
Second	30	0.005236	0.0308	0.4
Third	30	0.004416	0.0308	0.4
Fourth	30	0.0170442	0.0308	0.4

Fifth	20	0.004012	0.000308	0.4
Sixth	20	0.00561	0.000308	0.4
Seventh	20	0.00901	0.000308	0.4
Eighth	20	0.01309	0.000308	0.4

Table 4.1: Combinations of material properties of cohesive element

. At each and every time step energy release rate (G) is found by adding up the cohesive energy contributions from all N cohesive elements distributed in the finite element model Due to the use of variable σ_{max} and δ the cohesive energy spent in the N cohesive elements during crack growth has to be determined by integration

$$G = \sum_{i=1}^{N} \int (\sigma_n) d(u_n)_i \qquad i=1, N$$

where σ_n is calculated by the traction separation law [Eq2.1] where the integration over each element gives the cohesive energy spent in each element.

Above equation shows that energy release rate for propagation depends on the cohesive parameters viz. critical displacement jumps along the interface and maximum cohesive strength. So, by varying these parameters, fluctuations of energy release rate for propagation can be controlled.

The variation of energy release rate (G) with time is shown in Fig. 4.4.

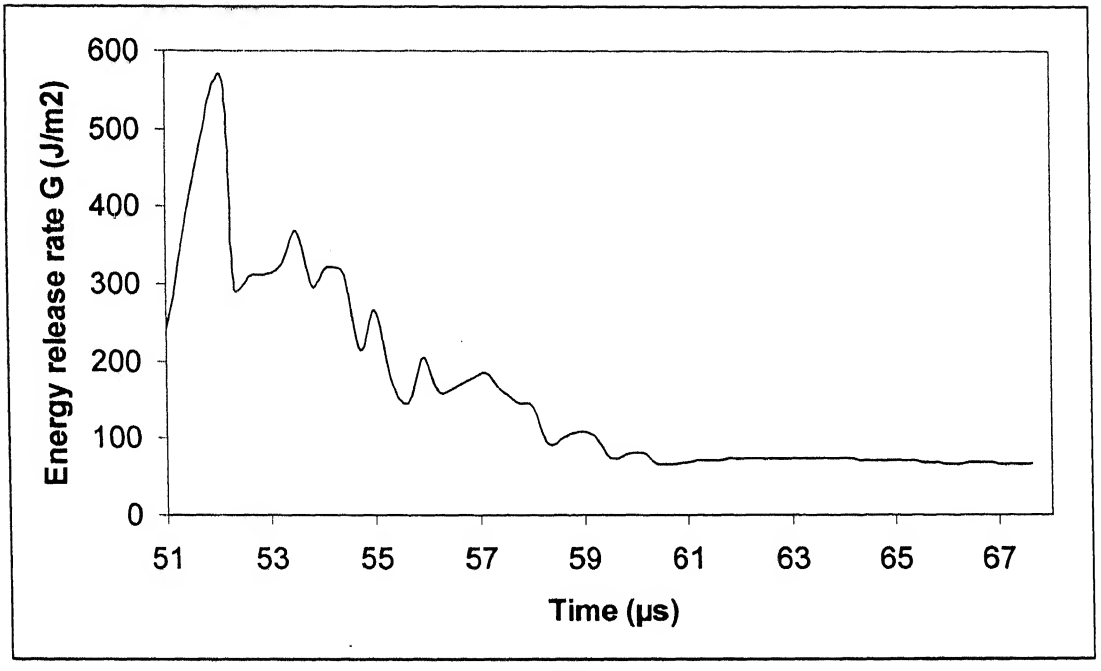

Fig 4.4 Energy release rate for steel specimen

At the crack initiation, energy is being consumed to create two new surfaces and due to that the energy release rate drops. As the crack advances, more and more new surfaces are formed and energy release rate shows a gradual decreasing nature. The present work follows the same trend for energy release rate curve.

Variation of energy release rate is such that it starts increasing up to the crack initiation point and then shows a smooth variation with small fluctuations at the inter-element boundaries.

The velocity of crack tip is calculated by taking the ratio of element size in crack propagation direction and the total time to cross that element. And it is observed that the propagation time taken to cross the first cohesive element is more than the second cohesive element and so on. Fig 4.5 shows that the crack propagation initiates with a low velocity and then increases as the propagation takes place. Variation of crack velocity with crack extension is shown in Fig 4.5.

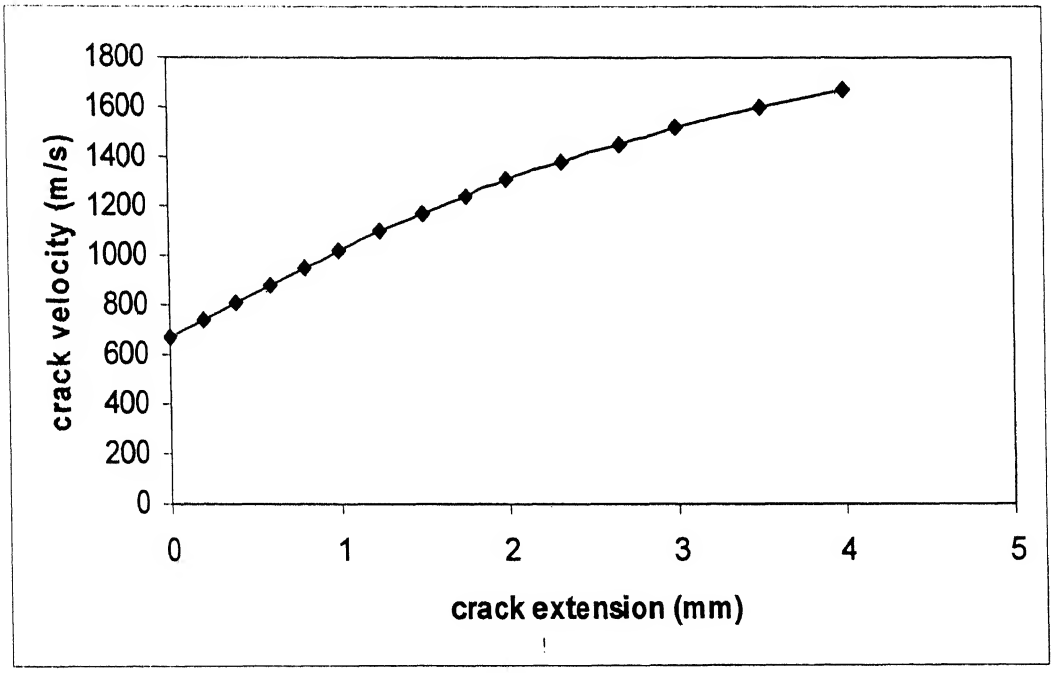

Fig 4.5 Crack velocity for steel specimen

4.3 Crack Propagation in Glass Fabric/Epoxy DCB Specimen

The present method is applied to determine the dynamic G_I for the experimental data as reported by Chowdhary [25] .

From the mechanics point of view fibre composites are among the class of material called orthotropic materials. Generalised Hook's Law for 2-D orthotropic laminate is given by Agarwal [31].

$$\sigma_{ij} = Q_{ij}\varepsilon_{ij} \tag{4. 1}$$

i,j=1,2....,6

where σ_i are the stress components, Q_{ij} is the stiffness matrix, ε_j are engineering strain components.

For 2-D orthotropic material,

$$\begin{Bmatrix}\sigma_1\\ \sigma_2\\ \tau_{12}\end{Bmatrix} = \begin{bmatrix}Q_{11} & Q_{12} & 0\\ Q_{21} & Q_{22} & 0\\ 0 & 0 & Q_{66}\end{bmatrix}\begin{Bmatrix}\varepsilon_1\\ \varepsilon_2\\ \gamma_{12}\end{Bmatrix} \tag{4. 2}$$

where,

$$Q_{11} = \frac{E_L}{1-\upsilon_{LT}\upsilon_{TL}} \tag{4. 3}$$

$$Q_{22} = \frac{E_T}{1-\upsilon_{LT}\upsilon_{TL}} \tag{4. 4}$$

$$Q_{12} = \frac{\upsilon_{TL}E_L}{1-\upsilon_{LT}\upsilon_{TL}} = \frac{\upsilon_{LT}E_T}{1-\upsilon_{LT}\upsilon_{TL}} \tag{4. 5}$$

$$Q_{66} = G_{LT} \tag{4. 6}$$

E_L and E_T are elastic modulus in longitudinal and transverse direction

G_{LT} is the shear modulus associated with longitudinal and transverse axes

υ_{LT} and υ_{TL} are major and minor Poisson ratios.

Relation between four of the five elastic constants is

$$\frac{E_L}{E_T} = \frac{\upsilon_{LT}}{\upsilon_{TL}} \tag{4. 7}$$

Following data is used as input for finding energy release rate.

- Displacement at cantilever end as a function of time
- Material data and specimen geometry

Material and geometric properties are as follows

- Material type — Glass fabric/epoxy laminate
- Material density — $\rho=1825 Kg/m^3$
- Elasticity constants — $E_L=26x10^9$ Pa
  $E_T=6.6x10^9$ Pa
  $G_{LT}=3.5x10^9$ Pa
- Poisson ratio — $\nu_{LT}=0.21$
  $\nu_{TL}=0.05331$

Two different experimental data is used.

Details of geometric data is given in Table 4.2

Table 4.2 Details of DCB specimen

Expt No	L(mm)	W(mm)	B(mm)	a (mm)
1	76	3.8	25.1	40.3
2	76	3.8	24.8	40.0

L – Length of the DCB specimen

W – Width of specimen

B – Thickness of specimen

a - Crack length

In the experiment 1, time history of displacement at the cantilever end is known. Fig 4.6 gives displacement applied at the cantilever end as a function of time. And this data is used as a input for finding dynamic energy release rate.

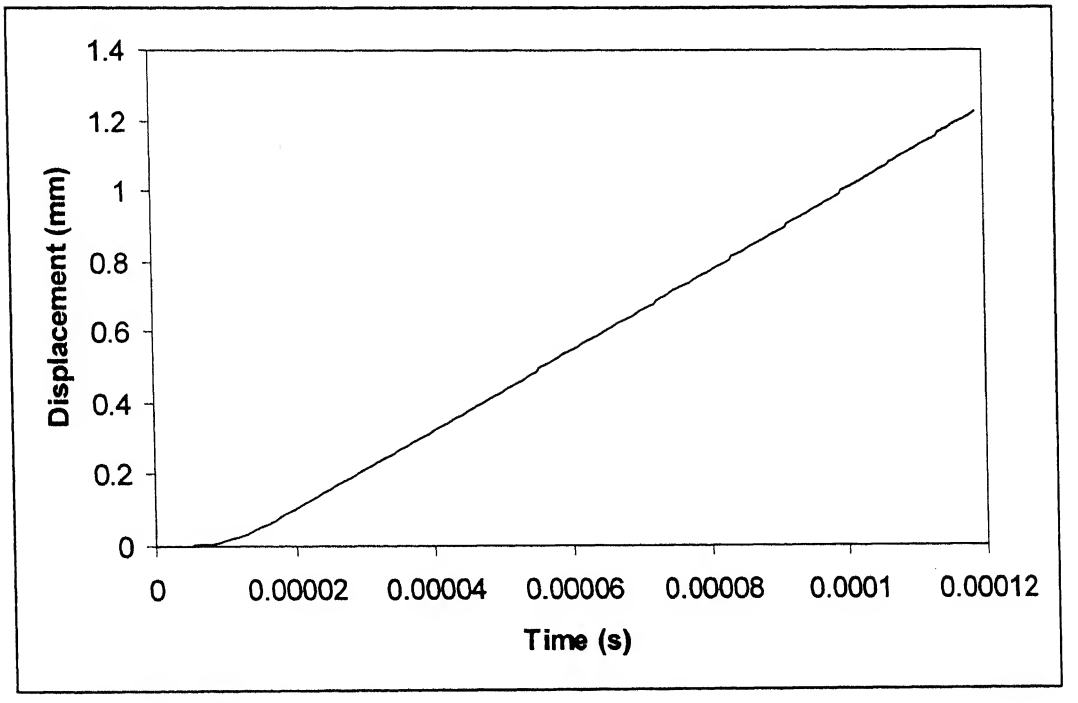

Fig 4.6 Displacement of the cantilever end (Experiment 1)

For determining the energy release rate following cohesive material parameters are taken for the experiments 1 [Table 4.3].

For the first cohesive element, choice of α_s, σ_{max} is made and the parameters δ_n, δ_s are chosen such that the energy release rates are matched with the experimental data (Chowdhary [25]). For the other cohesive elements these parameters are selected such that the energy release rate varies smoothly.

Elements	σ_{max} (MPa)	δ_n (mm)	δ_s (mm)	α_s
First	100	0.00175	0.0077	0.4
Second	10	0.0513366	0.002156	0.4
Third	10	0.0275366	0.000616	0.4
Fourth	10	0.0309366	0.000616	0.4
Fifth	10	0.0411366	0.000616	0.4
Sixth	10	0.0105366	0.000616	0.4
Seventh	10	0.0037366	0.000616	0.4

Table 4.3: Combinations of material properties of cohesive element for experiment 1

Energy release rate variation for experiment no 1 is shown in Fig 4.8. Similar results for force release model [25] is shown in Fig 4.7.

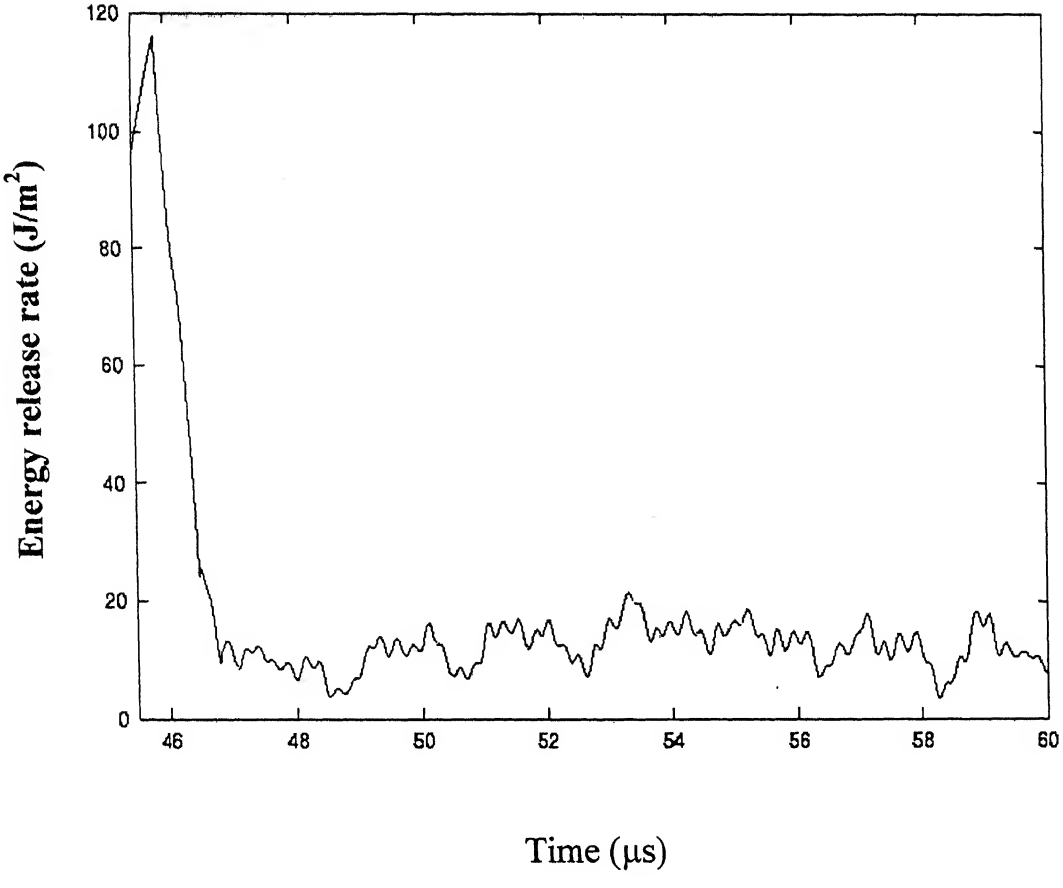

Fig 4.7 Energy release rate for Expt 1 [25]
By Force release model

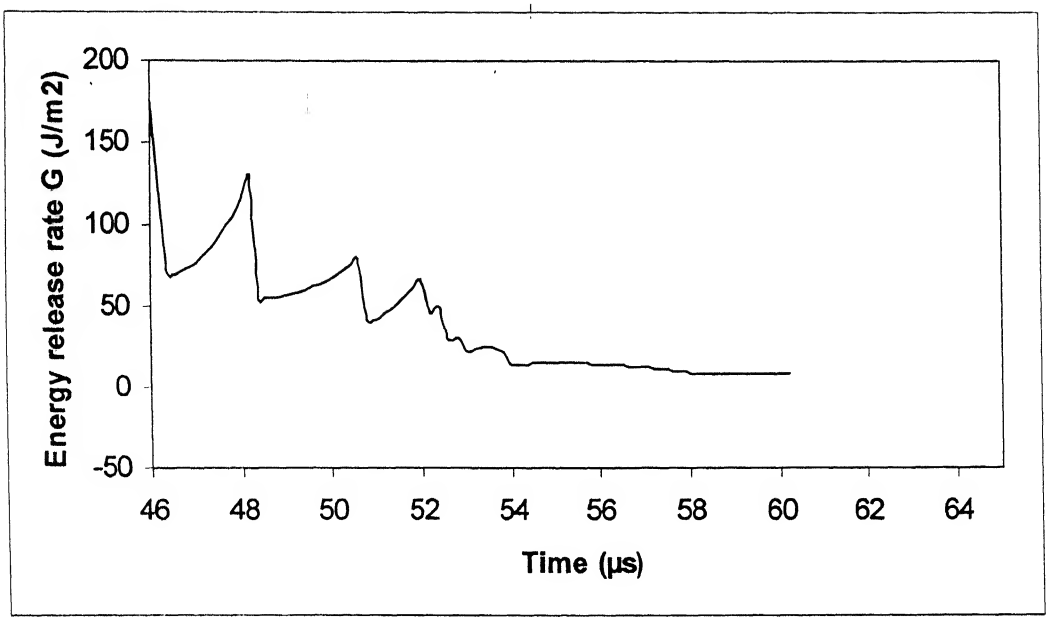

Fig 4.8 Energy release rate for experiment 1 (Present study)

At the crack initiation, energy is being consumed to create two new surfaces and due to that the energy release rate drops. As the crack advances, more and more new surfaces are formed and energy release rate shows a gradual decreasing nature. The present work follows the same trend for energy release rate curve.

In the present work, the variation of energy release rate is such that it starts increasing with the time, reaches the maximum value at the crack initiation and then it falls slightly at the first inter-element boundary of the cohesive element. And after that it shows a continuously decreasing pattern with the small fluctuations at the inter-element boundaries. In the force release model energy release rate shows the same nature up to the crack initiation point but after that at the first inter-element boundary it falls to a great extent and thereafter it shows large fluctuations at the other inter-element boundaries.

The initial velocity of crack tip is calculated for first cohesive element and the final velocity is taken from experiment 1 (Chowdhary [25]). It is assumed that the crack is moving with constant acceleration during propagation. Crack tip velocity varies such that crack propagation initiates with a low velocity and then increases as the propagation takes place.

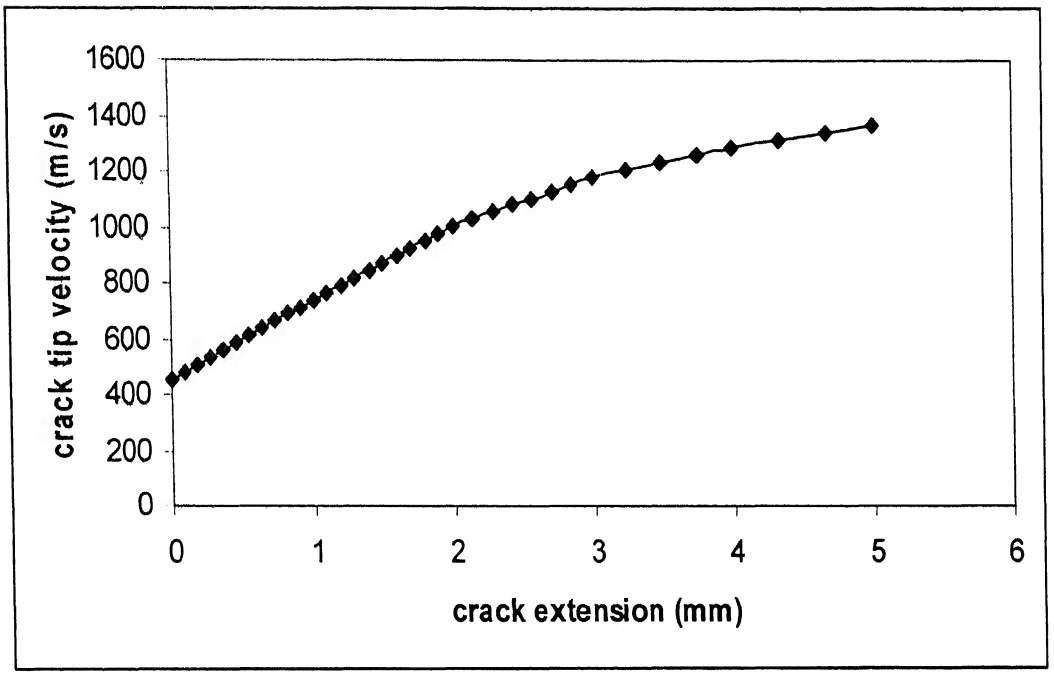

Fig 4.9 Crack tip velocity for Experiment 1

Fig 4.10 shows the variation of energy release rate with the crack tip velocity. As the crack propagation takes place energy release rate decreases with the crack tip velocity. At the low crack tip velocity energy release rate drops more and gradually it reduces at high crack tip velocity.

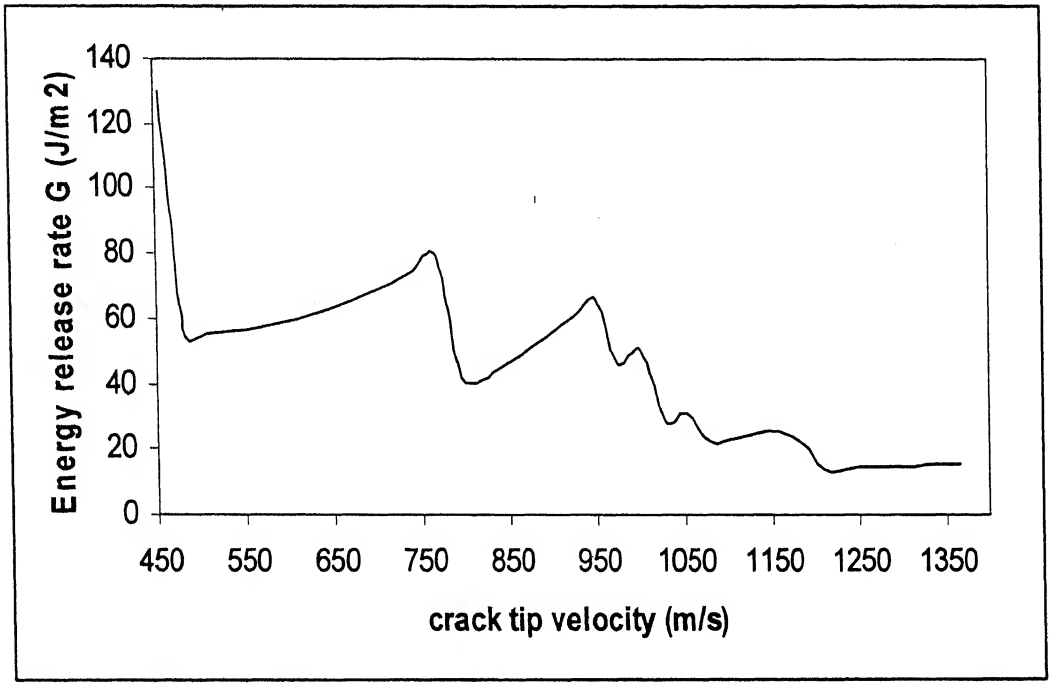

Fig 4.10 Energy release rate v/s crack tip velocity

Fig 4.11 shows the variation of energy release rate with the crack extension. As the crack propagation takes place, energy release rate increases within each elements and falls at the inter-element boundaries. Decrease in energy release rate at the inter-element boundaries reduces as the crack extension takes place as shown in Fig 4.11.

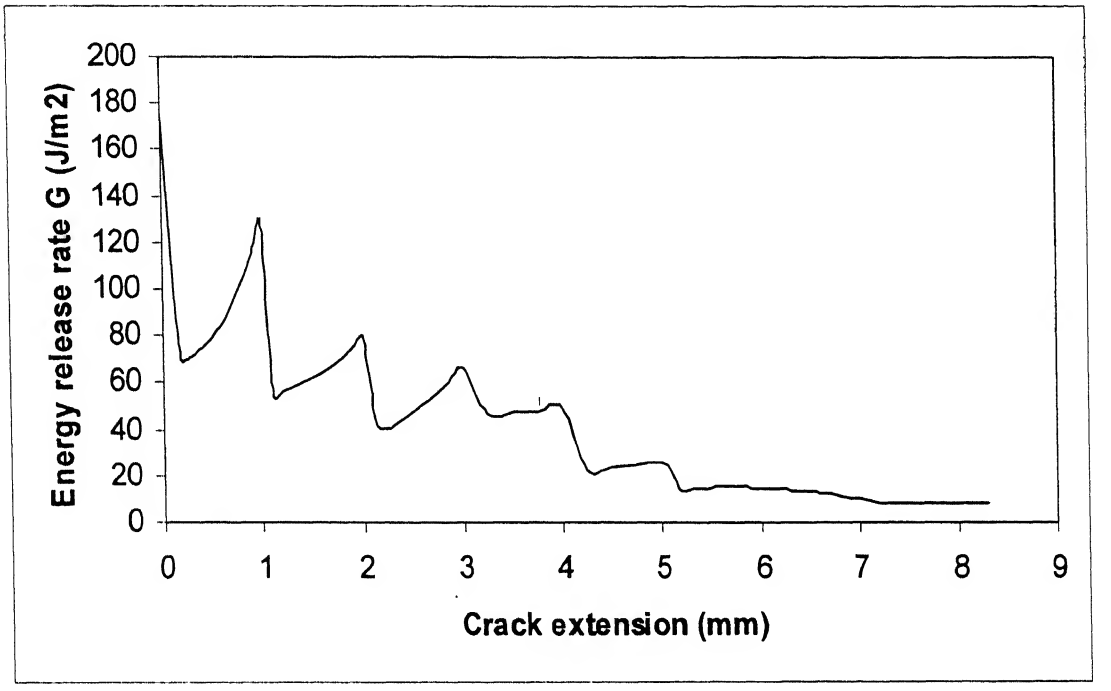

Fig 4.11 Energy release rate v/s crack extension

In the experiment 2, time history of displacement at the cantilever end is known. Fig 4.12 gives displacement applied at the cantilever end as a function of time. And this data is used as a input for finding dynamic energy release rate.

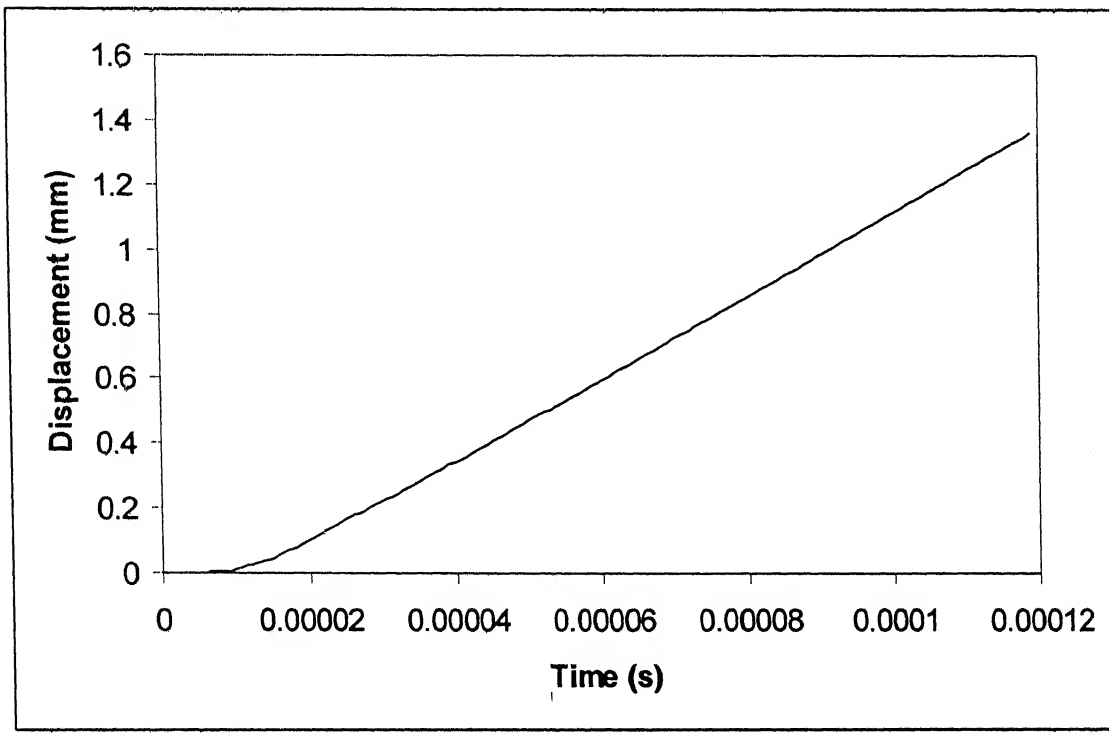

Fig 4.12 Displacement of the cantilever end (Experiment 2)

कलकर पुस्तकालय
भारतीय प्रौद्योगिकी संस्थान कानपुर
क्रमांक सं० A...152023

For determining the energy release rate following cohesive material parameters are taken for the experiments 2 [Table 4.4].

For the first cohesive element, α_s, σ_{max} and the parameters δ_n, δ_s are chosen such that the energy release rates match well with the experimental data (Chowdhary [25]). For the other cohesive elements these parameters are selected such that the energy release rate varies smoothly.

Elements	σ_{max} (MPa)	δ_n (mm)	δ_s (mm)	α_s
First	80	0.000233	0.001026	0.4
Second	30	0.00027166	0.000924	0.4
Third	10	0.0001428	0.000924	0.4
Fourth	10	0.00164628	0.000924	0.4
Fifth	10	0.00504628	0.000924	0.4
Sixth	10	0.01524628	0.000308	0.4
Seventh	10	0.02884628	0.00009548	0.4

Table 4.4: Combinations of material properties of cohesive element for experiment 2

Energy release rate variation for experiment no 2 is shown in Fig 4.14. Similar results for force release model [25] is shown in Fig 4.13.

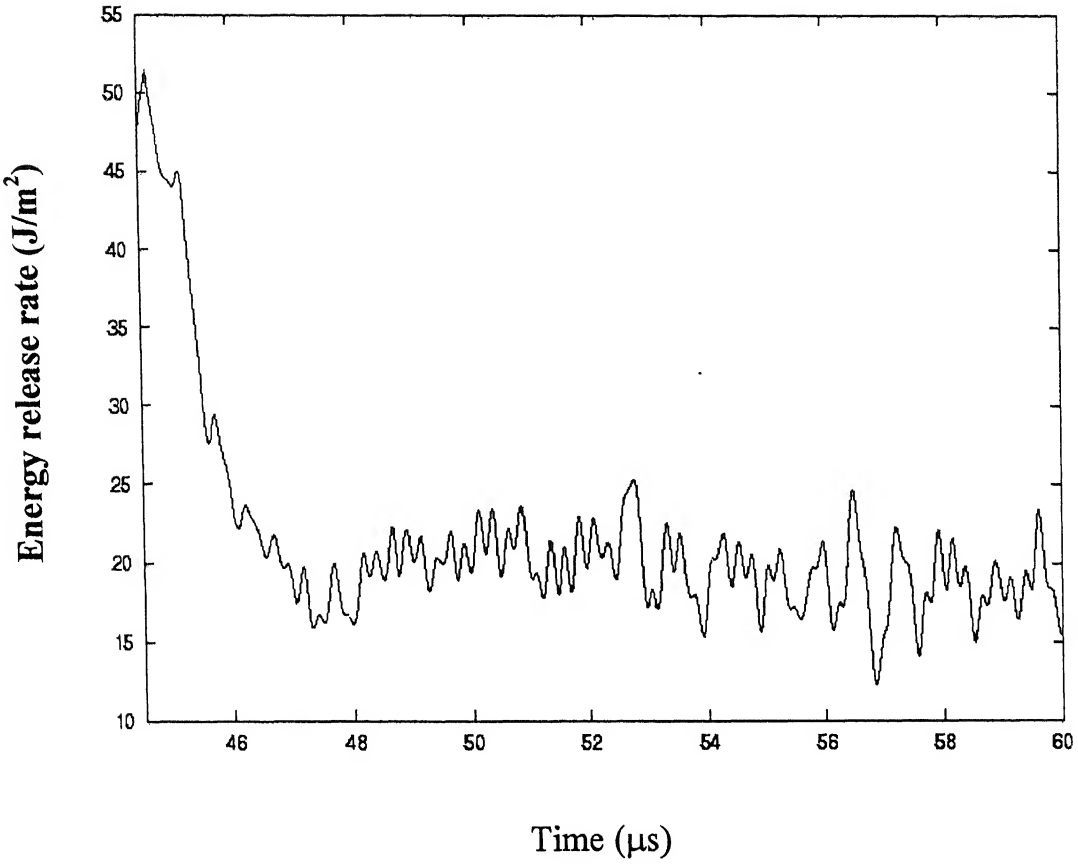

Fig 4.13 Energy release rate for Expt 2 [25]
By Force release model

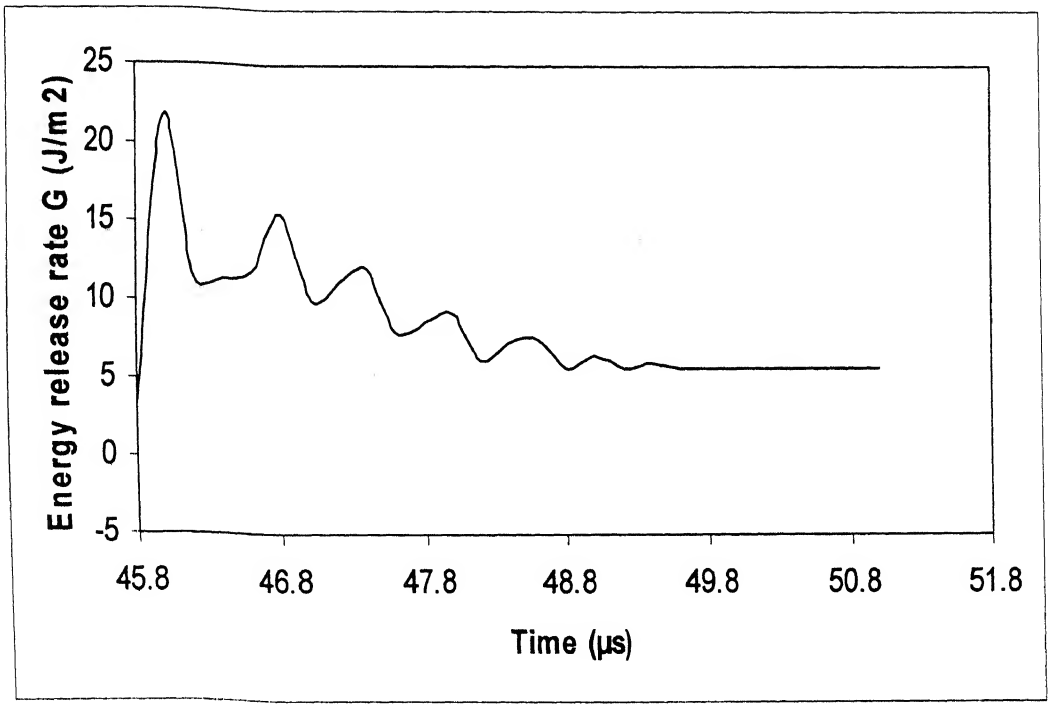

Fig 4.14 Energy release rate for experiment 2 (Present study)

At the crack initiation, energy is being consumed to create two new surfaces and due to that the energy release rate drops. As the crack advances more and more new surfaces are formed and energy release rate shows a gradual decreasing nature. The present work follows the same trend for energy release rate curve

For experiment 2 energy release rate curve for present method is shown in Fig 4.14, and it shows that the energy release rate increases till the crack initiates and then it slightly falls and then smooth variation of curve is shown with slight fluctuations as compared to the force release model [Fig 4.13].

The initial velocity of crack tip is calculated for first cohesive element and the final velocity is taken from experiment 2 (Chowdhary [25]). It is assumed that the crack is moving with constant acceleration during propagation. Crack tip velocity varies such that crack propagation initiates with some low velocity and then increases as the propagation takes place.

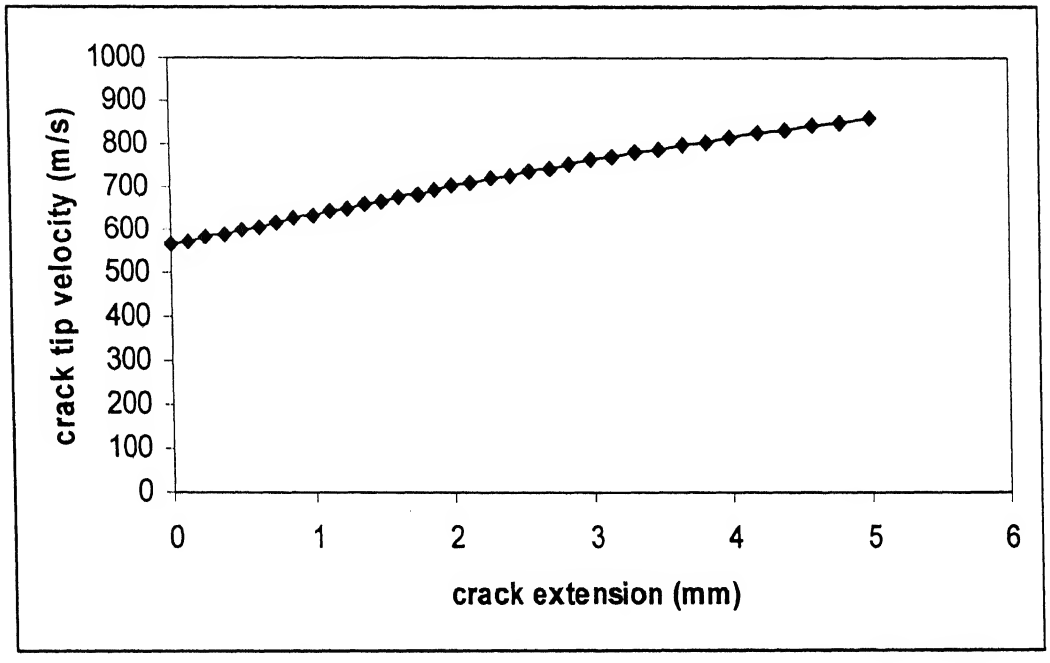

Fig 4.15 Crack tip velocity for Experiment 2

Fig 4.16 shows the variation of energy release rate with the crack tip velocity. As the crack propagation takes place energy release rate decreases with the crack tip velocity. At the low crack tip velocity energy release rate drops more and gradually it reduces at high crack tip velocity.

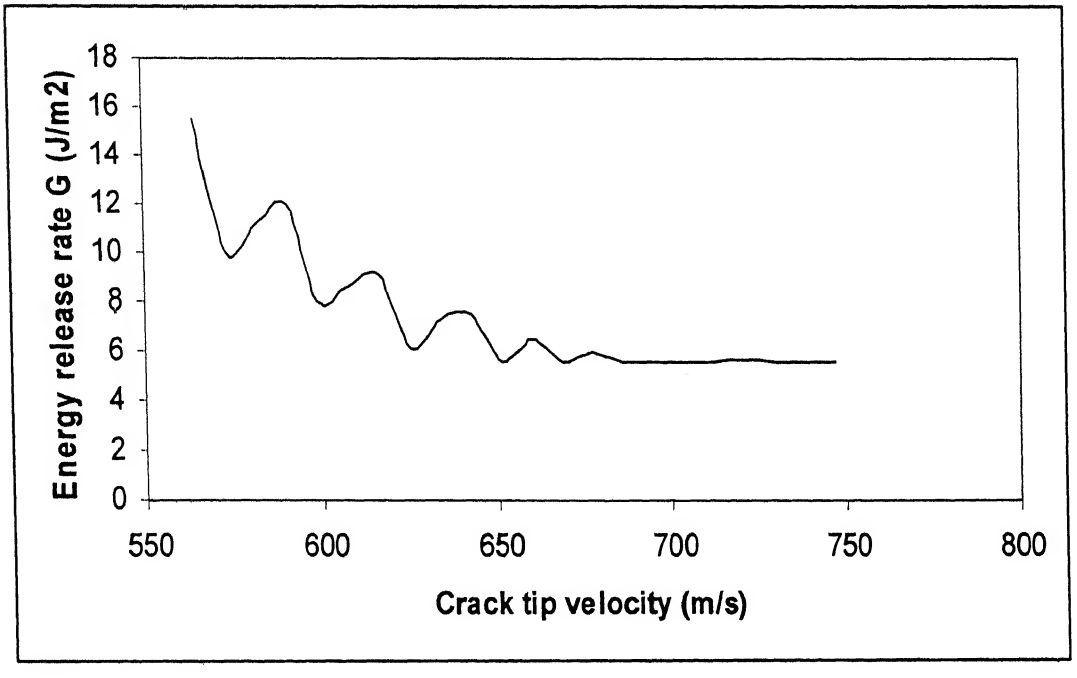

Fig 4.16 Energy release rate v/s crack tip velocity

Fig 4.17 shows the variation of energy release rate with the crack extension. As the crack propagation takes place, energy release rate increases within the cohesive elements and falls at the inter-element boundaries. Decrease in energy release rate at the inter-element boundaries reduces as the crack extension takes place as shown in Fig 4.17.

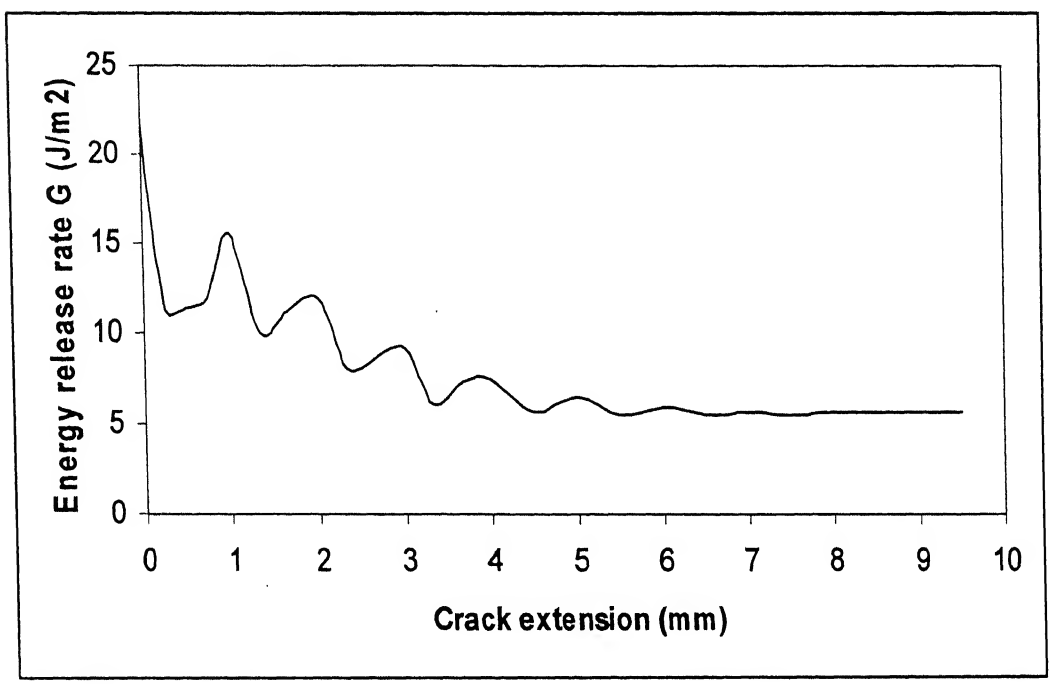

Fig 4.17 Energy release rate v/s crack tip velocity

Closure

In this chapter results for dynamic crack propagation analysis in DCB specimen is presented and discussed. The conclusions drawn from the above discussions are presented in the next chapter.

Chapter 5

Conclusions and Future Scope

In the present work the analysis of double cantilever beam is carried out. The delamination front is simulated for these cases. A parametric study of cohesive zone model for the DCB specimen is carried out. In this chapter the conclusions of the work are presented and future scope for the work is commented.

6.1 Conclusions

The conclusions are drawn as follows:

1. The delamination can be modeled and simulated as a crack nucleating and propagating along the interface of composite material laminae.

2. The delamination for a DCB specimen of glass epoxy composite material is simulated and is governed by mixed mode of crack propagation, with dominant mode I.

3. Model gives fairly smooth and more stable variation of energy release rate.

4. Experimental results reveal that unlike force release model energy release rate doesn't drop to a low value in very few time steps but falls gradually which is a more practical result.

6.2 Scope for Future Work

1. The crack propagation model may be further modified by modifying the cohesive properties to get more stable and smooth variation of energy release rate.

2. Cohesive zone model can be extended for the mixed mode analysis of composite materials.

3. This method can also be extended to delamination analysis for 3-Dimensional crack propagation problems.

Bibliography

1. Camanho P. P., Mathews F.L., Stress analysis and strength prediction of mechanically fastened joints in FRP: a review, Composites: Part A,(1997), 436-445.
2. Luciano R., Raffaele Z., A micromechanical approach for the analysis of damage in laminated composite structures, Computers and structures, Vol. 74, (2000), 201-214.
3. Phillips M.L., Yoon C., Allen D.H., A computational model for predicting damage evolution in laminated composite plates, Transaction of the ASME, vol.121, (1999), 436-445.
4. Barrenblatt G.L., The mathematical theory of equilibrium cracks in brittle fracture, Advance Applied Mechanics, vol.7,(1962), 55-129.
5. Dugdale D.S., Yielding of steel sheets containing slits, Journal of Mechanics and Physics of Solids, vol.8,(1960), 100-104.
6. Needleman A., A continuum Model for void nucleation by inclusion debonding, Journal of Applied Mechanics, vol. 54,(1987), 525-531.
7. Needleman A., An analysis of tensile decohesion along an interface, Journal of Mechanics and Physics of Solids, vol.38, (1990a), 289-324.
8. Needleman A., An analysis of decohesion along an imperfect interface, International Journal of Fracture, vol.42, (1990), 21-40.
9. Needleman A., Micromechanical modeling interfacial decohesion, Ultra microscopy, vol.40, (1992), 203-214.

10. Xu X.P., Needleman A., Numerical simulations of fast crack growth in brittle solids, Journal of Mechanics and Physics of solids, vol. 42 No.9, (1994), 1397-1434.
11. Tvergaard V., Fiber debonding and breakage in a whisker-reinforced metal, Material Science Engg. A 190, (1995), 215-222.
12. Tvergaard V., Hutchinson J.W., The relation between crack growth resistance and fracture process parameters in elastic-plastic solids, Journal of Mechanics and Physics, vol.40 No.6,(1992), 1377-1397.
13. Li H, Chandra N, Analysis of crack growth and crack tip plasticity in ductile materials using cohesive zone models, International Journal of Plasticity, vol. 19,(2003), 849-882.
14. Chandra N., Li H., Shet C., Ghonem H., Some issues in application of cohesive zone models for metal ceramic interface, International Journal of Mechaincs and Physics of Solids, vol. 39, (2002), 2827-2855.
15. EI-Sayed S., Sridharan S., Predicting and tracking interlaminar crack growth in composites using a cohesive layer model, Composites: Part B, vol.32, (2001), 545-553.
16. Crisfield M.A., Nonlinear finite element analysis of solids and structures vol.1, Willy Chichester, (1991).
17. Freund L.B., Dynamic Fracture Mechanics, Cambridge University Press, (1998).
18. Reddy J.N., An introduction to finite element method, McGraw-Hill, New York, (1993).
19. Zienkiewicz O.C., Taylor R.L., The finite element method forth edition vol.1, McGraw-Hill, London,(1989).
20. Talreja R., Transverse cracking and stiffness reduction in composite laminates, Journal of Composite Materials, vol.19, (1985), 355-375.
21. http://www.matweb.com/search/SearchSubcat.asp
22. Zhang Z., Paulino G.H., Cohesive zone modeling of dynamic failure in homogeneous and functionally graded materials, International Journal of Plasticity, vol. 21, (2005),1195-1254.